

The Geological Society of America Bulletin

An exceptionally long paleoseismic record of a slow-moving fault: the Alhama de Murcia fault (Eastern Betic Shear Zone, Spain)

--Manuscript Draft--

Manuscript Number:	B30558R2
Full Title:	An exceptionally long paleoseismic record of a slow-moving fault: the Alhama de Murcia fault (Eastern Betic Shear Zone, Spain)
Short Title:	Paleoseismicity of the AMF-southern tip
Article Type:	Article
Keywords:	paleoearthquake chronology; splay-structure; Quaternary geomorphology; Infrared Stimulated Luminescence (IRSL); fault segmentation.
Corresponding Author:	Maria Ortuño, Ph.D. Universidad Nacional Autonoma de Mexico Queretaro, Queretaro MEXICO
Corresponding Author's Institution:	Universidad Nacional Autonoma de Mexico
First Author:	Maria Ortuño, Ph.D.
Order of Authors:	Maria Ortuño, Ph.D. Eulalia Masana, Dr. Eduardo García-Meléndez, Dr. José Martínez-Díaz, Dr. Petra Štěpančíková, Dr. Pedro P. Cunha, Dr. Reza Sohbaty, Ph.D. student Carolina Canora, Dr. Jan-Pieter Buylaert, Dr. Andrew S. Murray, Dr.
Manuscript Region of Origin:	
Abstract:	<p>Most catastrophic earthquakes occur along fast moving faults although some of them are triggered by slow moving ones. Long paleoseismic histories are infrequent in the latter faults. An exceptionally long paleoseismic record (more than 300 ka) of a slow moving structure is presented: the southern tip of the Alhama de Murcia fault (AMF, Eastern Betic Shear Zone), characterized by morphological expression of current tectonic activity and by a lack of historical seismicity. At its tip, the fault divides into a splay with two main faults bounding the Góñar fault system. At this area, the condensed sedimentation and the distribution of the deformation in several structures provided us with more opportunities to obtain a complete paleoseismic record than at other segments of the fault. The tectonic deformation of the system was studied by an integrated structural, geomorphological and paleoseismological approach. Stratigraphic and tectonic features at six paleoseismic trenches indicate that old alluvial units have been repeatedly folded and thrust over younger ones along the different traces of the structure. The correlation of the event timing inferred for each of these trenches and the application of an improved protocol for the Infrared Stimulated Luminescence (IRSL) dating of K-feldspar allowed us to constrain a paleoseismic record as old as 325 ka. A minimum of 6 possible paleoearthquakes of Mw= 6 - 7 and a maximum mean recurrence interval of 29 ka were identified. This provided compelling evidence of the underestimation of the seismic hazard in the region.</p>
Suggested Reviewers:	Pilar Villamor, Dr. Manager, Institute of Geological and Nuclear Sciences, New Zeland P.Villamor@gns.cri.nz

	<p>She is an expert in paleoseismology and focused a part of her research on slow moving active faults</p> <p>Pablo Silva, Dr. Professor, Universidad de Salamanca, Spain pgsilva@usal.es His Ph.D thesis included the neotectonics of the study area of this manuscript. Also, he has performed several of the paleoseismological studies discussed in this manuscript.</p> <p>Tom Rockwell, Dr. Professor, San Diego State University trockwell@geology.sdsu.edu He has a wide background on the paleoseismological study of faults, which include faults in the Iberain Peninsula. Among his main research interest are earthquake histories and neotectonics.</p>
<p>Opposed Reviewers:</p>	
<p>Response to Reviewers:</p>	<p>All the minor changes suggested by the Associated Editor have been incorporated to the revised version of the manuscript.</p> <p>We would like to add a short comment to the following changes:</p> <p>1)line 290 "channel" for "river path" and delete "the" before Bermeja and "the" before Casas.</p> <p>response: We have removed the article "the" before the name for all the "creeks" throughout the manuscript, we have also replaced "path" or "drainage path" by "channel".</p> <p>2)line 302 "thinner conglomerate?" what is meant by this?</p> <p>response: We wanted to say small-size (fine) conglomerate, but since no size is specified in the description of the other material, we have remove it. It's not relevant for that description.</p> <p>3)line 309 how can hills formed by activity on the fault be displaced by it?</p> <p>response: We have clarified this issue by adding: "This displacement is probably related to the folding of the fault trace, so that the NE-SW oriented segment has a major strike-slip component, whereas the ENE-WSW segment is active as a major reverse fault"</p> <p>4)line 361 'extruded backwards'? What is meant by this?</p> <p>response: To clarify this matter, we have change slightly the sentence: "The Góñar faults, located between these faults dip steeply to the NE so that they probably merge at depth into the SAMF (Fig. 3). The blocks bounded by the Góñar faults have been uplifted to accommodate the shortening in the area"</p> <p>5)line 489 replace "by" with "as"</p> <p>response: Besides replacing "by" with "as", we have realized that there was an error in this sentence, which has been corrected as follows: "The age of these two events can only be constrained as predating unit C1 (at the Era trench, 149 – 135 ka pIRIR) and postdating the unit before unit B, unit Q at Gabarrones (274 – 242 ka pIRIR)"</p>

Cover Letter

[Click here to download Cover Letter: Cover_letter.pdf](#)

1 **An exceptionally long paleoseismic record of a slow-moving**
2 **fault: the Alhama de Murcia fault (Eastern Betic Shear**
3 **Zone, Spain)**

4 María Ortuño ^{a,b}, Eulalia Masana ^b, Eduardo García-Meléndez ^c, José
5 Martínez-Díaz ^d, Petra Štěpančíková ^e,
6 Pedro P. Cunha ^f, Reza Sohbaty ^g, Carolina Canora ^d, Jan-Pieter
7 Buylaert ^g, Andrew S. Murray ^g

8 *^a Centro de Geociencias, Universidad Nacional Autónoma de México, Blvd.*
9 *Juriquilla, 3001, 76230, Juriquilla, Querétaro, México*

10 *^b RiskNat group, Dep. de Geodinàmica i Geofísica, Universitat de Barcelona, Martí*
11 *i Franquès s/n, 08028 Barcelona, Spain*

12 *^c Área de Geodinàmica Externa, Facultad de Ciencias Ambientales, Universidad.*
13 *de León, Campus de Vegazana, s/n, 24071 León, Spain*

14 *^d Dep. de Geodinàmica, Universidad Complutense de Madrid, C/ Jose A. Novais*
15 *28040 Madrid, Spain*

16 *^e Institute of Rock Structure and Mechanics, Academy of Sciences of the Czech*
17 *Republic, V Holešovičkách 41, 18209 Prague 8, Czech Republic*

18 *^f Dep. of Earth Sciences, IMAR-Marine and Environmental Research Centre,*
19 *Universidade Coimbra, Largo Marquês de Pombal, 3000-272 Coimbra, Portugal*

20 *^g Nordic Laboratory for Luminescence Dating, Dep. Earth Sciences, Aarhus*
21 *University, Risø DTU, DK-4000 Roskilde, Denmark*

22
23 ** Corresponding author. Tel.: Tel.: +52 (442) 238-1104 Ext. 104; fax: +52 (442)*
24 *238-1124. E-mail address maria_ortuno@geociencias.unam.mx (M.Ortuño)*

25

26 **Abstract**

27 Most catastrophic earthquakes occur along fast moving faults although some of them
28 are triggered by slow moving ones. Long paleoseismic histories are infrequent in the
29 latter faults. An exceptionally long paleoseismic record (more than 300 ka) of a slow
30 moving structure is presented: the southern tip of the Alhama de Murcia fault (AMF,
31 Eastern Betic Shear Zone), characterized by morphological expression of current
32 tectonic activity and by a lack of historical seismicity. At its tip, the fault divides into a
33 splay with two main faults bounding the Góñar fault system. At this area, the
34 condensed sedimentation and the distribution of the deformation in several structures
35 provided us with more opportunities to obtain a complete paleoseismic record than at
36 other segments of the fault. The tectonic deformation of the system was studied by an
37 integrated structural, geomorphological and paleoseismological approach.
38 Stratigraphic and tectonic features at six paleoseismic trenches indicate that old
39 alluvial units have been repeatedly folded and thrust over younger ones along the
40 different traces of the structure. The correlation of the event timing inferred for each of
41 these trenches and the application of an improved protocol for the Infrared Stimulated
42 Luminescence (IRSL) dating of K-feldspar allowed us to constrain a paleoseismic
43 record as old as 325 ka. A minimum of 6 possible paleoearthquakes of $M_w = 6 - 7$ and
44 a maximum mean recurrence interval of 29 ka were identified. This provided
45 compelling evidence of the underestimation of the seismic hazard in the region.

46

47

48 *Keywords:* paleoearthquake chronology; splay-structure; Quaternary geomorphology;
49 Infrared Stimulated Luminescence (IRSL); fault segmentation.

50

51 **1. Introduction**

52 The identification and characterization of seismogenic faults are essential in
53 areas without historical damaging seismicity, which is common in tectonic regions with
54 low deformation rates.

55 The largest possible number of seismic cycles should be analyzed in order to
56 better understand the seismic behavior of a fault. Given the length of the cycles of slow
57 moving faults (tens of thousands of years), the study of these faults entails long
58 paleoseismic histories (hundreds of thousands of years). Our study is one of the few
59 works to date that provide a long record of slow moving faults.

60 Slow moving faults are more difficult to investigate than fast moving ones
61 owing to their muted morphological expression and to the difficulty of obtaining and
62 analyzing a long paleoearthquake record. The latter drawback is not only related to the
63 time-range of applicability of the current dating methods but also to the technical
64 impracticality of excavating very deep trenches. If the seismic activity of a slow moving
65 fault is recorded on condensed sedimentary sequences (which are related to moderate to
66 low sedimentation rates), trenches of only 2-3 meters depth can provide a paleoseismic
67 record of hundreds of thousands of years. We present an example of an exceptionally
68 long paleoseismic record of a slow moving fault affecting a condensed sedimentary
69 alluvial sequence: the southern tip of the Alhama de Murcia fault (AMF).

70 In the Iberian Peninsula, the historical seismic record (ca. 700 years) is much
71 shorter than the common recurrence interval of the Iberian seismogenic faults (> 5.000
72 years). The AMF is a slow moving fault with strong morphological expression of
73 activity but with no record of historical surface rupturing earthquakes. Nevertheless, on
74 May 11th 2011, after the conclusion of this study, the AMF produced the most

75 destructive earthquake in the Iberian Peninsula since 1881 (Andalusian earthquake, 25
76 December, EMS I = X; IGN, 2010). This M_w 5.1 event left thousands of people
77 homeless and claimed 9 fatalities in Lorca. The large number of people affected and the
78 considerable economic loss caused by this moderate earthquake were mainly due to a
79 shallow focus and a high peak acceleration of the ground in the most populated areas,
80 which had been underestimated in the national seismic hazard plans. The recorded
81 magnitude was much lower than the maximum expected magnitude ($M > 6$) proposed in
82 this work and in earlier paleoseismic studies in different segments of the AMF (Silva et
83 al. 1997; Martínez-Díaz, 1998; Martínez-Díaz et al., 2001, 2003; Masana et al., 2004).
84 This fault could therefore cause much more damage in the future.

85 We present the results of a thorough geomorphological, structural and
86 paleoseismic study carried out at the southern tip of the AMF in the proximity of Góñar
87 (**Fig. 1**). We focused on this area for the following reasons: 1) it is an instrumental
88 seismic gap; 2) there are no paleoseismic studies of this segment of the fault and 3)
89 some of its geomorphological, sedimentological and geodynamical characteristics
90 favour the preservation of a more complete paleoseismic record than adjacent segments.

91 We employed an improved method of luminescence dating to K-feldspar grains
92 based on elevated temperature infrared stimulated luminescence (post-IR IRSL or
93 pIRIR) dating (Sohbati et al., 2011 and references therein). This method, described in
94 section 3, allowed us to constrain much older palaeo-earthquakes than those previously
95 dated by quartz optically stimulated luminescence (OSL) dating. The combined use of
96 these methods provided us with an exceptionally long paleoearthquake record. The
97 novel geochronological methodology could be useful in the study of surface processes
98 and Quaternary geology.

99 In section 6, we highlight the significance of the results in terms of 1) the
100 characteristic rupture of the faults under study 2) the segmentation of the fault system
101 during seismic events and 3) the tectonic style in the study area. The unusually long
102 paleoearthquake history is analyzed together with the histories obtained from earlier
103 studies along other sectors of the AMF and Albox faults. This comparison offers new
104 insights into the seismotectonic behavior of the faults in the Eastern Betic Shear Zone,
105 which will have a considerable impact on seismic hazard assessment.

106

107 **2. Geological setting**

108 The AMF is located in the eastern part of the Betic Cordillera, the northern
109 branch of the Rif-Betic alpine orogenic belt, which resulted from the early Cenozoic
110 collision between the African and Eurasian plates. The Present-day relative plate motion
111 has been estimated as 4.5-5.6 mm/a (De Mets et al., 1994; McClusky et al., 2003).
112 Within the Iberian margin, a large part of the shortening is accommodated by faults in
113 the Eastern Betics Shear Zone (EBSZ) and by internal deformation (Masana et al.,
114 2004). Faults in the EBSZ (Bousquet, 1979; Banda and Ansorge, 1980; Sanz de
115 Galdeano, 1990) are mainly left-lateral strike slip structures oriented N-S to ENE-
116 WSW. Active faults in the EBSZ are the AMF, Carboneras, Palomares, Carrascoy, Bajo
117 Segura and San Miguel faults (Fig. 1a). All these faults are located in the internal zone
118 of the Betic range, where the basement consists of a stack of tectono-metamorphic
119 complexes (Nevado-Filbride, Alpujárride and Malaguide complexes; **Fig. 1**). In the
120 eastern part of the range, the tectonic exhumation of these complexes during the main
121 post-collisional period gave rise to a series of marine-continental tectono-sedimentary
122 basins (Sanz de Galdeano and Vera, 1992; Rodríguez-Fernández and Sanz de Galdeano,
123 1992; Montenat, 1996). Most of these basins were bounded by extensional faults.

124 Subsequently, Neogene to Present-day tectonics reactivated many of these faults, giving
125 rise to new intramontane sedimentary basins (Montenat and Ott d'Estevou, 1996,
126 Bardají, 1999).

127

128 *2.1. The Alhama de Murcia Fault*

129 The AMF is the longest fault in the EBSZ. First described by Montenat (1973) and
130 Bousquet and Montenat (1974), this fault has been considered to be one of the most
131 active faults in the Eastern Betics based on Quaternary geodynamical,
132 geomorphological and paleoseismologic data (e.g. Silva, 1994; Silva et al., 1992a, 1993,
133 1997; Martínez-Díaz, 1998, Martínez-Díaz et al., 2001; 2003; Masana et al., 2004). The
134 tectonic activity of the AMF since the Middle Miocene is characterized by oblique left-
135 lateral reverse kinematics (Montenat and Ott d'Estevou, 1996; Martínez-Díaz, 1998).

136 The Plio-Quaternary AMF extends from Alcantarilla to Lorca, along a ca. 100
137 km fault trace according to recent neotectonic studies (e.g. Silva et al., 1997, 2003;
138 Martínez-Díaz, 1998; Martínez-Díaz et al., 2003; Masana et al., 2004; Meijninger,
139 2006) although longer lengths have been proposed in earlier studies (e.g. Gauyau et al. ,
140 1977; Montenant et al., 1987) (**Fig. 1a**).

141 The AMF has been divided into different segments on the basis of its tectonic-
142 geomorphological features, its geodynamical evolution, its subsurface geometry and its
143 historical and present-day seismicity (Silva et al., 1992a; 2003; Martínez-Díaz, 1998).
144 To these criteria, Martínez-Díaz et al. (2010) add the paleo-seismic record and
145 distinguish four segments, from N to S: Alcantarilla-Alhama (25 km); Alhama-Totana
146 (11 km); Totana-Lorca (20 km); Lorca-Góñar (40 km) (**Fig. 1b**). To the SW of the
147 Lorca-Góñar segment, the AMF Plio-Quaternary activity is transferred to the Albox
148 fault (Masana et al., 2005), and possibly to other active structures described by some

149 authors (García-Meléndez, 2000; García-Meléndez et al., 2003, 2004; Meijinger, 2006;
150 Pedrera et al., 2010).

151

152 *2.2. Historical and instrumental seismicity*

153 Since the beginning of the historic seismic catalog in the Iberian Peninsula, at around
154 1300 A. D. (IGN, 2010), some regions have experienced moderate to large earthquakes.

155 Although the AMF is characterized by moderate to low ($M_w < 5.5$) instrumental
156 seismicity, it has been identified as the possible seismogenic source of at least six

157 damaging earthquakes occurring in 1579, 1674 (three of them), 1818 and 2011. These
158 events produced the maximum Medvedev-Sponheuer-Karnik intensities (MSK, very

159 similar to MMI) between VII and VIII in Lorca in the central-southern part of the AMF

160 (**Fig. 1b**). In the southern part of the AMF, a lack of historical and instrumental

161 seismicity has been observed by Silva et al. (1997), Martínez-Díaz (1998) and Masana

162 et al. (2004), among others. Although other faults in the area (such as the Palomares or

163 the Albox fault) also reveal an absence of damaging historical earthquakes and a weak

164 microseismicity (**Fig. 1b**), they have been shown to be seismogenic faults by means of

165 paleoseismic studies (Silva et al., 1997; Masana et al., 2005).

166

167 *2.3. Earlier paleoseismic surveys in the region*

168 In the proximity of Góñar, seven paleoseismologic sites have been studied: *La*

169 *Carraclaca*, *El Saltador*, and *El Colmenar* sites along the AMF in the surroundings of

170 Lorca; *El Ruchete* and *Urcal* sites at the Albox fault; and *Aljibejo* and *Escarihuela* sites

171 at the Palomares fault. The main structural and paleoseismic results of these studies are

172 summarized in **table 1** (see **Fig. 1b** for site location) and are discussed in this paper.

173 Most of the deformation observed in the paleoseismic studies listed in **table 1**
174 prompted the authors (from Silva et al., 1997; Martínez-Díaz et al., 2003; García-
175 Meléndez, 2000; García-Meléndez et al., 2004; Soler et al., 2003; Masana et al., 2004;
176 Masana et al., 2005) to assign earthquake magnitudes of up to $M= 6 -7$ to the seismic
177 events recorded in the trenches.

178

179 **3. Methods**

180 We studied the geomorphology and structure of the southern tip of the AMF
181 with the aid of aerial photographs (scale: 1:33.000 and 1:18.000) and field
182 reconnaissance and mapping using ortho-images and 1:10.000 topographic maps. A
183 paleoseismic study was performed at six trenches in the Góñar fault zone (**Fig. 2**). All
184 the trenches were 2-3 m deep with the exception of *Carrascos-1*, which is a natural
185 outcrop on the northern margin of *Carrascos* creek. At this site, ca. 0.5 m of material
186 was scraped off the wall to clean the exposure. The trenches varied in length (from 18 m
187 to 50 m) and were all excavated perpendicularly to the fault trace, except *Carrascos-1*,
188 which was slightly oblique to it. We installed a 1 m grid (2 m locally at the *Carrascos-1*
189 and *Tio Rey* trenches) and used photo-mosaic and graph paper to log the paleo-
190 deformation recorded at the trenches.

191

192 *3.1 Dating of Quaternary units*

193 Dating deformed units is essential for constraining the age of the paleoearthquakes and
194 for calculating the slip rates attributed to each of the faults. The age constraints in this
195 work were derived from quartz thermoluminescence (TL) dating and K-feldspar
196 elevated temperature infrared stimulated luminescence (p-IRIR) dating of sediments.
197 The results of the dating are given in **table 2**.

198

199 *K-Feldspar post IR IRSL (pIRIR) dating*

200 The material sampled for dating consists of fine sand or mud with a high concentration
201 of felsic minerals. One of the advantages of analyzing K-feldspar is that older samples
202 can be dated given that its luminescence signal can grow to doses that are much higher
203 than those for quartz. However, the luminescence signal from K-feldspar is not often
204 thermally stable (this phenomenon is called anomalous fading) with the result that
205 special care must be taken to evaluate and correct the loss of signal during the burial
206 time of the sample.

207 An improved protocol of infrared stimulated luminescence (IRSL) dating of K-
208 feldspar based on those proposed by Thomsen et al. (2008) and Buylaert et al. (2009)
209 was followed to obtain the accumulated doses in the samples from paleoseismic
210 trenches at Góñar. Radionuclide concentrations were measured by high-resolution
211 gamma spectrometry to estimate the dose rate. In the p-IRIR dating procedure (see
212 Sohbaty et al. 2011), the IRSL signal is measured at an elevated temperature (e.g. 225° C
213 for 100 s) after an infrared bleach at a low temperature (e.g. 50° C for 100 s). K-feldspar
214 p-IRIR fading corrected ages were considered to be the best age estimates of the
215 samples.

216

217 **4. The southern tip of the AMF: the AMF-Góñar fault system**

218 The southern tip of the AMF represents the tectonic boundary between the *Las*
219 *Estancias* range (uplifted block) and the *Guadalentin* and *Huerca-Overa* basins
220 (downthrown block) (**Fig. 1b**). The Plio-Quaternary infill of these basins mainly
221 consists of siliciclastic alluvial fans and minor fluvial system deposits and carbonate
222 rocks. These deposits overlie a folded and faulted sequence of marine marl with inter-

223 bedded conglomerate and evaporite of the Late Miocene (Briend, 1981; Silva, 1994;
224 Martínez-Díaz, 1998; García-Meléndez et al., 2003). The Late Miocene and Plio-
225 Quaternary rocks in this area are part of a fan-like structure interpreted as a cumulative
226 wedge or progressive unconformity (García-Meléndez et al., 2003). The geological
227 units exposed at the *Las Estancias* range consist of a Permian and older metamorphic
228 basement (mainly schist, phyllite and marble) and a sedimentary cover. The cover is of
229 Miocene age and contains mainly red conglomerate inter-bedded with silt, sand and
230 evaporite (Voermans et al, 1978) (**Fig. 2**).

231 The geomorphology of the northeastern and southwestern parts of the study area
232 has been mapped by Silva (1994) and Silva et al. (1992b), and by García-Meléndez
233 (2000), respectively. The Quaternary active deformation of the Góñar area has
234 previously been reported only by Briend (1981), who addressed local deformation of
235 Quaternary alluvial fans affected by reverse faulting and by folding with a 070°- 080 °
236 axis trend. These Quaternary alluvial fans overlie late Miocene marls and turbidites in
237 the *El Judio* creek (**Fig. 2**). According to Briend, the reverse faults offset the Quaternary
238 deposits by a few meters.

239 **Figure 2** shows the main geomorphological units of the area and the traces of
240 the main structural features. Morphological and sedimentary features such as alluvial
241 fans, slope deposits, fluvial terraces and faceted spurs were mapped. We classified the
242 Quaternary alluvial fans as G0 (for the deposits of the Present-day active drainage) to
243 G6 (for the oldest recognizable alluvial fan). In most cases, the younger alluvial fans are
244 incised in the older ones in an off-lap depositional style. This entrenching of the alluvial
245 system seems to be closely related to the ongoing tectonic uplift of the area. Some
246 alluvial fans are locally blocked in the distal area by the tectonic uplift of blocks in the

247 *Guadalentín* basin. The distal part the alluvial fans has an anomalous rectilinear shape
248 where this blockage occurs.

249 The southern tip of the AMF at Góñar forms a splay-like structure termed the
250 AMF-Góñar fault system. This system of faults is made up of a) two boundary faults,
251 the northern AMF (NAMF) and the southern AMF (SAMF), and b) several internal
252 structures, known as the Góñar faults (strands 1, 2, 3 and 5, henceforth, FS1 to FS5).
253 The minimum length of the fault splay is ca. 6 km. This value might be an
254 underestimation of the real length because it was calculated from the geomorphological
255 mapping where the morphology of Quaternary alluvial fans is preserved (**Fig. 2**). To the
256 SW, the Quaternary faulting is not evident since only sub-vertical Miocene-Pliocene
257 strata crop out along the *Garita del Diablo* structural high (**Fig. 1b**) and no clear
258 geomorphological markers are preserved.

259 Two main features make the AMF-Góñar fault system more suitable than the
260 northernmost segments of the AMF for the preservation of a complete paleoseismic
261 record. First, the fault zone is made up of several strands of oblique to parallel faults.
262 This configuration is more suitable for the record of paleoearthquakes than fault
263 segments with a single trace and with a continuous orientation. This is attributed to the
264 greater spatial coverage associated with a wider fault zone, which is usually related to a
265 larger variety of erosive and sedimentological environments than a discrete fault zone.
266 Second, the orthogonal orientation of some parts of AMF-Góñar fault system with
267 respect to the NW-SE convergence between the African and Iberian plates gives rise to
268 more vertical displacements than the northernmost fault segments. This maximum
269 vertical slip compensates for the small slip per event at the tips of fault systems.

270

271 *4.1 The northern Alhama de Murcia fault (NAMF)*

272 The northern structural boundary of the AMF-Góñar structure, i.e. NAMF, consists of a
273 single (locally double) trace and defines the *Las Estancias* range front in the study area.
274 The fault affects Miocene red sand and conglomerate, and to a lesser degree, Plio-
275 Quaternary conglomerate (**Fig. 2**). Near the *El Judío* creek, the NAMF is characterized
276 by a centimetric dark gray and yellow fault gouge. The fault plane has a 030°/70°-80°
277 NW orientation and slickenlines with a 55° pitch to the SW. These data and the
278 geomorphology of the area indicate that the NW block of the NAMF is being uplifted
279 with a south-eastward component. At the northern end of the study area, the NAMF is a
280 20-30 m wide fault zone consisting of three fault strands. Two fault orientations were
281 observed in this fault zone; 015°/60°-70° NW and 040-060°/80° NNW. Minor secondary
282 faults with a 100°/ 85° N orientation and showing slickenlines with a pitch 80° to the W
283 were identified.

284 The strongest evidence for Quaternary deformation along the NAMF includes
285 faceted spurs along part of the range front, and the left lateral deflections of the older
286 channels of *Bermeja* and *Casas* creeks. In both creeks, the old channel to the SE of the
287 fault was displaced clockwise and was abandoned. The channel abandonment was
288 probably related to a capture process linked to headward erosion of the creek to the SW.
289 The left strike-slip deflections of the channel are 359 ± 14 m at *Bermeja* creek and 417
290 ± 26 m at *Casas* creek (**Fig. 2b**). It was not possible to undertake a paleoseismic study
291 of this fault because of the absence of Plio-Quaternary depositional units and
292 geomorphological markers that could be correlated on both sides of the NAMF trace.

293

294 4.2 The southern Alhama de Murcia fault (SAMF)

295 The SAMF is the southern boundary fault of the AMF-Góñar structure. Its activity has
296 produced an elongated tectonic high, the *La Gata* hills, parallel to the NAMF trace

297 (Figs. 2 and 3). The strata in the *La Gata* hills form a cumulative wedge (or progressive
298 unconformity) representing the northeastern continuation of the *La Garita del Diablo*
299 topographic high, described by García-Meléndez et al. (2003). Beds forming the wedge
300 dip to the SE at angles ranging from 80° (Neogene marls) to 60°- 50° (Plio-Quaternary
301 conglomerate) and 30° (possibly Early Pleistocene limestone and conglomerate).

302 The SAMF crops out at site 3 (Fig. 2a), and is covered by Quaternary sediments
303 to the NE of *La Gata* hills. The fault was identified as a 5-8 m wide fault zone with a
304 060°-070°/85° N orientation showing slickenlines with a 5°-10° pitch to the SW (Fig.
305 4k). The fault zone is characterized by a fault breccia and a fault gouge and by a local
306 and sudden change in the dip of the conglomeratic beds, which are interpreted as part of
307 rotated blocks. The continuation of the SAMF to the N can be inferred by the left lateral
308 offset of 1) the *La Gata* hills, displaced by ca.1 km in the out-wash zone of the *Fraille*
309 and *Bermeja* creeks. This displacement is probably related to the folding of the fault
310 trace, so that the NE-SW oriented segment has a major strike-slip component, whereas
311 the ENE-WSW segment is active as a major reverse fault and 2) two adjacent creeks
312 (channels b and c in Fig. 5) between *Carrascos* and *Yesos* creeks, which are displaced
313 by 127 ± 6 m and 77 ± 10 m. The Present-day configuration of the drainage network in
314 this area suggests that the southernmost creek was displaced and then captured by a
315 straighter channel (channel a), resulting in the abandonment of part of the channel,
316 which was displaced towards the NE (channel b).

317 Another fault with a 020°/80°NW orientation and slickenlines pitching 30° to the
318 north was observed a few meters to the SE of the SAMF outcrop along the main road to
319 Góñar (site 3, Fig. 2a). The fault cuts Plio-Quaternary bioclastic and brecciated
320 limestone. Another fault can be observed at a quarry in the neighborhood (site 4, Fig.
321 2a).

322 The fault has a reverse component that can be deduced from the apparent
323 vertical displacement of the alluvial fan G5 (ca.1 m; Fig. 4i). It is not possible to
324 ascertain whether the fault continues to be active because of the agricultural
325 transformation of the land.

326

327 4.3 The Góñar fault system

328 The Góñar fault system is located between the NAMF and the SAMF. The splay
329 consists of sub-parallel fault strands trending NNE-SSW (FS 1 to 5 in Figs. 2a and 3).
330 The faults are almost vertical or dip steeply towards the SE, parallel to the Neogene
331 strata in most cases. In the southern part, the Góñar fault system consists of two strands
332 (FS4 and FS3). In the northern part, next to the linkage with the NAMF, the Góñar fault
333 system made up of of three strands (FS1, FS2 and FS3). FS2 has an associated antithetic
334 fault forming a push up structure. Other minor faults offset the Quaternary alluvial fans
335 by only a few centimeters and are considered secondary structures. Further details of the
336 Góñar fault system are discussed below on the basis of the paleoseismological analysis.

337 The combined activity of the Góñar faults and the SAMF has given rise to a
338 wide anticline (the Góñar anticline) deforming Miocene and Plio-Quaternary strata (Fig.
339 2, Fig. 3). This structure has at Present the shape of a stripped anticline, resulting in the
340 outcrop of the underlying Miocene basement (Fig. 4c and d). The high erodability of
341 the outcropping marls lead to the formation of an elongated erosional depression
342 (between the *La Gata* hills and the *Las Estancias* range in Fig 2a). This depression
343 acted as a trap for the Quaternary alluvial fans, which have been deformed locally by
344 the Góñar fault system. Recent activity of the fault system was only detected where
345 Quaternary deposits are preserved.

346

347 *4.4 Structure at depth*

348 **Figure 3** shows a sketch of the main structures observed in the area and their
349 hypothetical continuation at depth. The proposed model regards the structure as a
350 compressional bend between the NAMF and the SAMF. Part of the Quaternary
351 deformation in this compressional zone occurs in the Góñar fault system.

352 The opposite dip of the NAMF and SAMF with respect to the Góñar faults
353 suggests complexity at depth. The NAMF dips to the NW and is left-lateral reverse with
354 the result that the northwestern block is uplifted to the SE. This geometry and
355 kinematics are consistent with geomorphological and structural data reported for the
356 contiguous northern segments (Silva et al., 1997, 2003; Martínez-Díaz, 1998;
357 Meijninger, 2006). By contrast, the faults in the Góñar fault system dip steeply to the
358 SE and have a reverse component with an uplifted southeastern block (**Fig. 2a, Fig. 3,**
359 **and Fig. 6**).

360 The SAMF is almost vertical at the surface and probably dips more gently to the
361 NW at depth, where it probably merges into the NAMF. The Góñar faults, located
362 between these faults dip steeply to the NE so that they probably merge at depth into the
363 SAMF (**Fig. 3**). The blocks bounded by the Góñar faults have been uplifted to
364 accommodate the shortening in the area.

365 The SAMF may be assumed to be a detachment zone below the Góñar fault system. The
366 displacement of the Middle-late Quaternary channels, which is attributed to this fault
367 (**Fig. 5**), attests to its recent activity. This accounts for the progressive tilting of
368 Neogene and Plio-Quaternary layers that make up the cumulative wedge that crops out
369 at the *Garita del Diablo* and *La Gata* hills (**Fig. 1** and **Fig. 2**).

370

371 **5. Trenching analysis**

372 Our paleoseismic study focused on the Gonar fault system, owing to multiple
373 sites showing deformation of middle-late Quaternary cover, in contrast to the absence of
374 Quaternary deposits overlying the traces of the NAMF and SAMF (**Fig. 2a**).

375 Six trenches were excavated on the strands of the Góñar system. Three of them
376 were located in the northern area on faults FS1, FS2 and FS3. The other three trenches
377 were placed in the central-southern part of the system on FS4 and FS5 (**Fig. 2a and Fig.**
378 **3**). Faulted alluvial fan deposits are exposed at the trenches. The source areas of the
379 alluvial fans are located on late Tortonian red conglomerate, cropping out along the
380 southeastern border of the *Las Estancias* range. Units P-J, Q, B and C1 at the trenches
381 correspond to the oldest alluvial fans (alluvial phases G4 to G6). The youngest alluvial
382 phases (G0 to G3) are represented by units C2-3 and D (**Fig. 2, Fig. 6 and Table 2**).
383 These units are folded and faulted, giving rise to tectonic highs that blocked the
384 youngest alluvial fan deposits, which are also locally deformed, albeit to a lesser degree.

385 The following sections present the descriptions of the trenches. The stratigraphy
386 of the units observed at the trenches is summarized in the legend in **figure 6. Table 2**
387 compiles the facies interpretation of each unit and its TL and pIRIR ages. The pIRIR
388 age was used whenever a unit was dated through TL and pIRIR methods in order to
389 provide the most uniform chronology.

390 At each trench, different markers were used to measure the deformation along
391 the exposed faults. We assigned an uncertainty value (ranging from 2% to 21% of the
392 mean value) to the displacement values measured in each case. This value depended on
393 the degree of clarity of the contact. Only one measurement had a much larger
394 uncertainty, this being almost 50% of the mean value.

395 A minimum of 15 events (summarized in **table 3**) were identified, some of
396 them possibly corresponding to the same earthquake observed at different trenches.

397 The identification of the events was based on **1)** the fault displacement of the Present
398 day soil, **2)** the sealing of a fault by a younger unit, **3)** the displacement of a fault by
399 another fault, **4)** the angular unconformity between two adjacent units, **5)** a sudden
400 change in the sedimentary conditions due to a possible tectonic origin and **6)** the
401 formation of a colluvial wedge interpreted as the collapse of a fault scarp.

402 The time range of each event was determined by using the ages of the postdating and
403 predating units at its trench (**Table 3**). At some cases, those ages were not available.
404 Then, we used the age for those units at the closest trenches.

405

406 *5.1 Carrascos site (strands 2 and 3)*

407 *Carrascos* corresponds to the area where the AMF changes from a single trace to a
408 splay of different fault strands. Two trenches separated by ca. 80 m were studied at
409 this site: *Carrascos-1* to the NE, and *Carrascos-2* to the SW (**Figs. 2, 3a, 6a, b and c**).
410 The activity of the faults has led to the formation of several hills blocking the alluvial
411 sediments of the small creeks to the SE of *Carrascos* creek.

412 Three depositional phases are observed at *Carrascos-1*: an older phase (G5)
413 represented by unit B, an intermediate phase (G4 and G3) consisting of units C1 to C3,
414 and a younger phase (G2) made up of units D1 and D2. These alluvial deposits are
415 overlain by a soil unit.

416 With the exception of the upper part of D1, all units are faulted and/or folded.
417 Four faults are exposed at the trench. The north-western fault corresponds to the Góñar
418 FS2, which dips ca.15° to the SE and displaces unit C and the base of D1 (**Fig. 6b**). The
419 other three faults correspond to FS3, and are termed fault *a*, *a'*, and fault *b*. Fault *a* is
420 vertical and faults *a'* and *b* dip 45° and 40° to the SE, respectively. Faults *a'*, *b* and FS2
421 have a fault-propagation fold associated with each of them. The degree of folding is

422 greater for the oldest units. Units D1 and D2 are gently folded. Only fault *a'* displaces
423 all the units. Adjacent to the faults, the clasts within the different beds are progressively
424 rotated and the beds of units B and C1 are stretched. Gouge is solely associated with
425 fault *a*, which is less than 20 cm thick. Faults *a'* and *b* match the axial plane of the fold
426 without a well defined fault plane. The dips of these faults suggest that they merge at
427 depth; faults *a* and *b* probably intersect at less than 10 m below the surface, and FS2 and
428 FS3, a few meters below this intersection.

429 At *Carrascos-2*, only units B and C and fault 2 are exposed. The units are
430 dragged and folded by FS2, which dips 55 ° to the SE and is continuous up to the
431 present-day surface. The fault is associated with an asymmetric anticline (affecting
432 unit B) in the upthrown block and a recumbent syncline (affecting units C2 and C3) in
433 the downthrown block (**Figs. 4 and 6c**). The fault is characterized by a white fault
434 gouge that is a few millimeters thick. Subhorizontal open fractures affect unit C1 next
435 to the fault, indicating the existence of subhorizontal compressional stress orthogonal
436 to the fault.

437

438 *Paleoseismic events*

439 Five events were identified at *Carrascos-1*, Ca-1 to Ca-5 from youngest to oldest.

440 The youngest event, **Ca-1**, was associated with FS2. This event displaces the base of
441 unit D2 (D2-1) but not the top (D2-2). The vertical displacement associated with this
442 event is 23 ± 11 cm. The only age constraint of this event is the age of unit D1 at the
443 *Gabarrones* trench, 21 - 25 ka TL, and the age of unit D3 at Era, 3.25- 3.89 ka TL.

444 Event **Ca-2** occurred on FS2 and FS3. Near FS2, the base of unit D1 and the
445 previous units are more folded than the upper part of unit D1 and the subsequent units.
446 The event occurred shortly after the deposition of the base of D1 and does not affect

447 its upper part. At this fault, this event produced a vertical displacement of 36 ± 4 cm.
448 At fault *b* (FS3), a deformation event led to the tilting of C3 and the underlying units,
449 whereas D1 unit overlying fault *b* was not deformed. The horizon of this event next to
450 fault *b* was placed below a colluvial unit interpreted as a tectonic colluvial wedge.
451 Both events were considered as the same event (Ca-2) because the base of unit D1
452 (deformed by FS3 during this event) was probably not deposited next to FS2 or was
453 removed by erosion after the earthquake. The accumulated vertical slip of these events
454 at the base of D1 is 60 ± 9 cm. Thus, this event would be bracketed by units C3 and
455 the middle part of D1. We selected the age of D1 at the *Gabarrones* site (21 - 25 ka
456 TL at *Gabarrones*), and not the age of D2 at the *Era* site (12 – 16 ka pIRIR at *Era*) as
457 the post-dating age since the former is likely to be closer to the time of faulting than
458 the latter. Summarizing, the age of Event Ca-2 can be constrained by C3 (46 – 60 ka
459 pIRIR) and D1 (21 - 25 ka TL at *Gabarrones*).

460 **Ca-3** is defined by a colluvial wedge formed next to fault *b*. This colluvial
461 wedge is made of clasts derived from unit C2, which was probably uplifted and
462 removed by erosion in the upthrown block. Additional evidence in support of **Ca-3** is
463 the intense red color (enhanced precipitation of ferrous minerals) at the base of unit C3
464 near the fault zone (**Fig. 4g**). This feature is interpreted as resulting from the formation
465 of an ephemeral pond at the toe of the scarp, possibly related to the obstruction of the
466 drainage caused by the co-seismic growth of the scarp.

467 The displacement associated with event Ca-3 is ca. 78 ± 6 cm. According to the
468 relationships proposed by McCalpin (1996), the vertical displacement associated with
469 one event is approximately twice the maximum thickness of a fault derived colluvial
470 wedge associated with it, in this case 39 ± 3 cm. Such a relationship is based on direct
471 observations made on present-day fault ruptures (McCalpin, 1996) and is based on the

472 fact that the co-seismic colluvial wedges are made of clasts derived from the rapid
473 degradation of the fault scarp after the earthquakes so that their maximum thickness
474 (i.e., the thickness next to the fault) is ca. a half of the original height of the scarp
475 before its collapse.

476 Another estimation of the vertical slip can be obtained from the displacement
477 of the base of C3 unit, 27 ± 5 cm. These slip values are a minimum estimate of the
478 total slip associated with such an event because it is an estimate of the vertical
479 displacement and only corresponds to one of the fault strands of the system. This event
480 occurred before the deposition of unit C3 (46 – 60 ka TL) and after a period of reduced
481 sedimentation postdating unit C2 (103 -126 ka TL). This is corroborated by a calcrete
482 layer on top of this unit and below the colluvial wedge.

483 Event horizon of **Ca-4** was located within subunit B2, whose upper part was
484 not affected by fault *a'*. Movement along fault *a'* displaced fault *a* and the beds in
485 subunit B1. Event **Ca-5** is indicated by faulting of subunit B1 and the basal part of B2.
486 The envelope surface of the B1/ B2 contact and of layers within B2 is displaced
487 vertically by 117 ± 8 cm. Given that this displacement is likely to be the result of at
488 least 4 events, a mean value of 23 ± 2 cm per event is obtained. It was not possible to
489 correlate the layers of unit B dated at *Carrascos-2* and the layers of unit B exposed at
490 *Carrascos-1*. The age of these two events can only be constrained as predating unit C1
491 (at the *Era* trench, 149 – 135 ka pIRIR) and postdating the unit before unit B, unit Q at
492 *Gabarrones* (274 – 242 ka pIRIR).

493 Events from Ca-1 to Ca-5 cannot be well constrained by the deformation of the
494 units exposed at *Carrascos-2*, where FS2 is exposed. Although the fault at this trench
495 extends up to the Present-day surface, no clear offset of the soil is observed. The
496 propagation of the fault plane into the soil could be due to an event more recent than

497 Ca-1. However, it could also be apparent and could result from an irregular
498 development of the soil over the fault zone. Since such a hypothetical event is not
499 observed at *Carrascos-1*, 80 m to the west, we did not to interpret this feature as a real
500 faulting of the soil. Consequently, all the events may have contributed to the formation
501 of the drag fold observed at *Carrascos-2*, although they cannot be well constrained.

502

503 *5.2 Gabarrones site (strand 1)*

504 The *Gabarrones* geomorphological setting bears a strong resemblance to that of
505 *Carrascos-2*. Here, the presence of a lighter colored topographic high on G6, delimits
506 the front of alluvial fan G2 (**Fig. 2**). A trench was excavated perpendicular to this
507 linear boundary between units G6 and G2, revealing the Góñar FS1. This fault strand
508 is also exposed at the *El Asno* creek with a 020-025/70° SE trend (slickenlines with 20°
509 S pitch). It has an associated shear zone affecting a well cemented conglomerate that is
510 probably of Middle Pleistocene age.

511 The deposits of alluvial fan phases (**Fig. 6d**) are folded and faulted in such a
512 way that **1**) the beds of unit Q dip ca.70° SE, **2**) intermediate units (B, C1 and C2) are
513 less folded and faulted, and **3**) the youngest units are slightly deformed (C3) or
514 undeformed (D1 and soil unit). The structure revealed at the trench corresponds to an
515 asymmetric syncline with a faulted sub-vertical southeastern limb (**Fig. 6d**). All the
516 faults in this limb merge at depth into a vertical fault (fault *a*) that represents the
517 southeastern boundary of the fault zone. The overall structure is interpreted as a tilted
518 push-up structure. This is supported by a lensoidal-shape defined by the faults in the
519 NE wall of the trench. Fault *b* has an orientation of 087°/25°S. The slickenlines on its
520 plane have a pitch of 70°W, indicating oblique reverse and left-lateral movement (**Fig.**
521 **4j**).

522

523 *Paleoseismic events*

524 Evidence for five events, Ga-1 to Ga-5 from youngest to oldest was found at this site.
525 The youngest event (**Ga-1**) tilted the synclinal structure to the NW, slightly folding
526 unit C3. This is evidenced by the geometry of the internal layering of C3, which dips
527 slightly to the SE and runs parallel to the contact between C3 and C2 except near the
528 fault zone, where it dips to the NW. Since C3 is an alluvial unit with a NE provenance,
529 the dip of its layers towards the NE is not expected to be a sedimentological feature. A
530 minimum of 129 ± 3 cm of vertical slip was inferred for this event by considering the
531 offset of the base of C3, which is observed in the downthrown block and can be set to
532 below the present day soil in the upthrown block. Tilting is likely to be tectonic and
533 cannot be ascribed to fault *b*, as unit C3 is not broken. The fault producing this tilting
534 could either belong to the group of faults located to the SE or could be another fault
535 not exposed at this trench and located more to the SE. This event occurred after the
536 deposition of C3 (47 – 51 ka pIRIR at *Carrascos-2*) and before unit D1 (21 - 25 ka
537 pIRIR).

538 The previous event, **Ga-2**, was caused by fault *b*, which cut the colluvial
539 wedge. The contact between the colluvial wedge and the over-riding block is a fault.
540 The uplifted part of the colluvial wedge was probably eroded away before the
541 deposition of C3 unit, which is expected since the top of the fault scarp would be made
542 of it.

543 The colluvial wedge consists of angular clasts derived from units C1 and B and
544 was formed during an earlier event, **Ga-3**. Using the McCalpin (1996) estimates of
545 displacement based on colluvial wedge thickness, we obtained a minimum vertical slip
546 of 75 cm for event Ga-3. The Ga-2 and Ga-3 events occurred after the deposition of

547 C2 (108 - 116 ka pIRIR ago) and before the deposition of C3 (47 - 51 ka pIRIR ago at
548 *Carrascos-2*). The ages obtained at these trenches do not allow us to distinguish a
549 different time constraint for these events.

550 The dip displacement of the Q-B contact along fault *b* is 103 ± 22 cm. This slip
551 probably results from at least two events, one producing the colluvial wedge and a
552 successive one displacing it. Then, a 51 ± 11 cm of dip displacement is attributed to
553 each of the events Ga-2 and Ga-3. A 116 ± 25 cm net slip per event was calculated
554 using the aforementioned measure and the orientation of the slickenlines of the fault.

555 Events **Ga-4** and **Ga-5** are related to the movement along fault *a* and along the group
556 of faults that merge into it. Event Ga-4 displaced unit B (174- 208 ka pIRIR at
557 *Carrascos-2*) but not unit C1 (100 -116 ka pIRIR) so that an event horizon was placed
558 at the base of unit C1. Event Ga-5 corresponds to the angular unconformity between
559 units Q and B. Layers in unit Q dip steeply to the SE with the result that more than one
560 event probably occurred between their formation (before 258 – 274 ka pIRIR) and the
561 deposition of unit B.

562

563 *5.3 Tio Rey site (branch 3)*

564 The *Tio Rey* site was chosen for excavation because of the anti-slope inflexion of the
565 alluvial fan surface that favors sediment trapping. The precise location of the faults in
566 the neighboring *El Asno* and *Los Yesos* creeks helped to locate the trench (**Fig. 2**). The
567 faults in the creek are oriented $060^{\circ}/70^{\circ}$ SE and have affected the Neogene marls and
568 the overlying Quaternary alluvial fans.

569 The *Tio Rey* trench only exposes the deposits of alluvial phase G6 (units P and
570 J in the trench log; **Fig. 6**). The units within the alluvial fan are part of a train of
571 synforms and antiforms affecting units P and J. In most of the trench, the layers do not

572 show their natural slope but are tilted towards the NW, i.e. facing uphill. These folds
573 have been cut by a series of reverse faults, most of them dipping SE (e.g.: *a*, oriented
574 058°/35 and *b*, oriented 060°/35SE) and one dipping NW (fault *c*; oriented
575 030°/45°NW). Fault *b* has slickenlines with a pitch of 80° W, indicating a reverse left
576 lateral component. The faults have discrete fault gouges consisting of well cemented
577 white silt. All the faults exposed at the trench are probably secondary faults associated
578 with the main faults observed at the *El Asno* creek.

579 We calculated the long term net slip accommodated by the exposed faults. To
580 this end, we undertook a microtopographic profile of the folded surface of alluvial fan
581 G6. The profile was perpendicular to the trace of FS4 and contained the trench (inset
582 of **Fig. 6e**). The base of unit J near the reference point X dips 7 ° to the SE, as in the
583 microtopographic profile in the NW sector. By extrapolating the Present-day surface
584 of G6 to the trench, we obtained a minimum vertical displacement of 3.24 ± 0.36 m of
585 unit J. This value is equivalent to the vertical displacement of 3.26 ± 0.36 m of this
586 unit associated with fault *b*, which corresponds to a dip slip of 6.72 ± 0.74 m. (**Fig.**
587 **6d**).

588

589 *Paleoseismic events*

590 We were only able to constrain one event at the *Tio Rey* trench, event **Tr-1**. The
591 movement along fault *b* has a major vertical component, as inferred from the
592 slickenlines and from the vertical offset of the units. This fault extends towards the
593 surface, and displaces the top soil unit by ca. 15 cm along the dip (**Fig. 4f**). Thus, an
594 event horizon was placed at the top of the soil unit (Tr-1). The age of this event is
595 uncertain. Given that the area is affected by natural erosion and by plowing, it is
596 debatable whether the soil affected by the fault is a modern one. A tentative Holocene

597 age has been assigned to event Tr-1 in accordance with the degree of soil
598 development.

599 A total offset of 6.72 ± 0.74 m along the dip on this fault suggests the
600 occurrence of some earlier earthquakes, identified as Tr-X, after the deposition of unit
601 P, i.e. after 290 ± 13 ka pIRIR.

602

603 *5.4 Sardinias site (branch 4)*

604 *Sardinias* trench is located at Góñar (**Fig. 2, Fig.6f**), on the trace of FS4. The site
605 corresponds to an asymmetric hill, with a maximum height of ca. 3 m on the steepest,
606 NW facing side. The exposure at this trench showed that the Neogene basement is
607 uplifted, blocking alluvial fans G3 and G2 sourced from the *Las Estancias* range.
608 During the deposition of G3, the alluvial fan overran the scarp as indicated by the
609 preservation of the G3 alluvial deposits (unit C3) at the top of the hill (**Fig.6f**).

610 The Neogene sequence at this site consists of an alternation of conglomeratic
611 beds (with rounded clasts) and marls dipping 80° SE. Units H to C3 dip to the NW,
612 and uncomformably overlie the basement. Units H1 and H2 consist of clasts embedded
613 in a pale silty matrix. The color and lithology of units H1 and H2 indicate that they are
614 derived from the Neogene basement exposed in the upper part of the trench. Units H1
615 and H2 are interpreted as colluvial units generated by the degradation of the *Sardinias*
616 scarp. Clast imbrications and lithology of alluvial units C2, C3 and D1 confirm that
617 they are sourced from the *Las Estancias* range.

618 FS4 consists of at least two fault strands, fault *a* and “inferred fault *b*”. The
619 Neogene sequence is affected by a 40 - 50 cm thick fault zone, i.e. fault *a*, which is
620 oriented $045/75^\circ$ SE and is parallel to the bedding. The fault gouge is characterized by
621 c-s structures indicating a dominant reverse movement with a minor left lateral

622 component. Deformation along fault *a* could have contributed to the progressive uplift
623 of the *Sardinas* hill in the past, but it did not affect the overlying deposits (unit H and
624 soil). Its location and orientation do not account for the folding of the overlying units
625 (H1 to C3), which must have been generated by movement along an inferred fault,
626 fault *b*. Deformation of the layers in the foot wall of fault *a* is expressed as an open
627 fold with the axial plane dipping to the SE and probably coincident with the inferred
628 fault *b*. Strong tilting of the layers to the NW is observed. The 10° dip in the central
629 part of the trench increases to 35° in the northwestern part. The uppermost unit, D1, is
630 the only non-deformed unit. The 6° dip of the layers to the SE is probably depositional
631 since it is coincident with the general slope of alluvial fan G2 obtained through
632 microtopography. The top of this unit has been transformed by plowing.

633

634 *Paleoseismic events*

635 Evidence of at least three paleoearthquakes was obtained at this site, Sa-1 to Sa-3 from
636 youngest to oldest. The youngest event observed, **Sa-1**, is defined by an angular
637 unconformity located at the base of unit D1'. This event also caused the uplift of part
638 of unit C3 located at the top of the hill. To estimate the minimum vertical offset
639 associated with this event, we assumed that the original surface of alluvial fan G3 had
640 the same slope as the surface of the undeformed alluvial fan G2, i.e. 6° to the SE.
641 Then, we restored the folding affecting unit C3 (alluvial fan G3) in the northwestern
642 block and projected its base underneath unit C3 in the southeastern block (**Fig. 6f**).
643 This projection suggests a minimum vertical displacement of 3.55 ± 0.39 m for the
644 base of C3. The age of this event is constrained by unit D1' (39 - 50 ka TL) and unit
645 C3 (59 - 63 ka pIRIR). Event Sa-1 probably corresponds to several events, as
646 suggested by the anomalously large throw of 3.55 m associated with it.

647 The identification of events **Sa-2** and **Sa-3** is based on the change in
648 sedimentary environment represented by the base of units H1 and H2, respectively. In
649 each of these earthquakes, the *Sardinas* hill would have been uplifted and the newly
650 exposed basement rock would have been rapidly eroded and deposited at the foot of
651 the scarp. The high erodability of the basement rocks suggests that the colluvial layers
652 (H1 and H2) were formed in a relatively short period after two events. Alluvial
653 sediments (C2) were deposited between this rapid sedimentation associated with H1
654 and H2. Thus, event Sa-2 should have occurred between units C2 and C3, i.e. between
655 59 ka and 159 ka TL. Event Sa-3 occurred before the deposition of C2 (99 -159 Ka
656 TL) so that a 99 ka TL age is considered as a minimum age for it
657 We did not consider the ages obtained for the H1 colluvial deposit since the distance
658 from the source was insufficient to ensure the total bleaching of the grains used for the
659 luminescence dating.

660

661 *5.6 Era site (branch 4)*

662 The *Era* site is located at Góñar, next to the head of a highly entrenched active creek
663 that provides a good exposure of the fault (site 6 in **Fig. 2a** and **Fig. 4e**). At the
664 surface, this site shows a gentle step of ca. 1 m, separating orchards (in the
665 downthrown block) from an abandoned threshing floor (in the upthrown block). In the
666 northwestern margin of the creek, the Góñar FS4 can be deduced from the sharp
667 contact between vertical Neogene marl in the hanging block and late Quaternary
668 alluvial deposits in the downthrown block. Another natural exposure of this fault can
669 be observed at site 1 (**Fig. 2**), where the layers of the alluvial fan G3 are folded and
670 thrust 0.5 m to the NW. The fault is oriented 055°/50° SE in the natural outcrop and
671 060°/25° SE at the trench.

672 Two faults are observed along the axial planes of the folds affecting the units
673 in the *Era* trench (**Fig. 6g**). Alluvial fan G5 (unit B2) is overlain by alluvial fan G3
674 (unit C1), both being folded and thrust towards the N-NW over alluvial fans G3
675 (unit C1 to 3) and G2 (units D2 and D3). This deformation caused an antiformal fold
676 in the over-thrusting block and a synformal fold in the downthrown block. The faults
677 exposed are more easily identified in the units with a well cemented matrix (as the
678 upper part of C1 and C2), where discrete fault planes can be observed. However, in the
679 units that are clast supported, the fault can only be inferred from the alignment of the
680 clasts. Small offsets of ca.10 cm were observed within unit C1 and at the C1-C2
681 contact. The overall structure bears a strong resemblance to that exposed at *Carrascos*
682 1 and 2 trenches (**Fig. 6a**). A vertical displacement of 4.68 m associated with this fault
683 was estimated by considering the C1-B contact in the upthrown block and its estimated
684 depth at the downthrown block. The contact was drawn taking into account the
685 maximum thickness of C1 observed underneath the fault (**Fig. 6g**). This is a minimum
686 estimate of the vertical slip since the base of unit C1 is probably located at a lower
687 position.

688

689 *Paleoseismic events*

690 At this trench, it was possible to constrain only one event, **Era-1**, at the top of unit C3.
691 Unit C3 is folded in contrast to unit D3, suggesting that the event occurred after C3 (at
692 this trench, 55 – 61 ka pIRIR) and before the deposition of unit D3 (3.25 – 3.89 ka
693 TL). Since it was not possible to ascertain whether D2 was deformed, it is debatable
694 whether this event occurred before the deposition of unit D2. However, the fact that
695 D2 was not preserved on the hanging block suggests that unit D2 was uplifted during
696 event Era-1 and was subsequently eroded away. We used the age of C3 as the

697 maximum age for this event, although it should be borne in mind that this event could
698 be younger than D2. The top of C3 is therefore considered to be the paleosurface after
699 this event (**Fig. 6g**).

700

701 **6. Discussion**

702 In this section, the timing of the events obtained for the six paleoseismologic
703 trenches is compared to obtain the correlation of the events, i.e. the common event
704 chronologies that could account for the deformation at the different sites. The slip rates
705 derived from the trench analysis are also discussed. The results are compared with the
706 event chronologies and slip rates of the neighboring paleoseismological sites studied
707 by other authors. This comparison allows us to evaluate the maximum fault rupture
708 inferred from the correlation of the events, and to provide some estimates of the
709 maximum magnitude expected in the region. Finally, some geodynamical implications
710 are discussed at the end of the section.

711

712 *6.1 Correlation among the paleo-seismic events at the Goñar faults*

713 We used the term “paleoearthquake” (abbreviated to PE) for the paleoseismic events
714 derived from the correlation between different trenches while the term “events” is
715 restricted to those identified by a single trench analysis (e.g., Ca-1, etc.). The summary
716 of the age constraints and slips associated with all the events is provided in **table 3**.
717 The correspondence between each event and the common PE is given in this table. The
718 PEs are listed 1 to 6, from youngest to oldest.

719 A minimum of 6 PEs were inferred. This is a minimum estimate of the PEs
720 recorded at the trenches since we cannot be sure whether all the earthquakes were
721 recorded. In the oldest units, the deformation attributed to a single event is possibly the

722 result of two or more successive events. In the case of folds, it is not easy to interpret
723 the deformation in terms of the number of events. The same thing occurs when
724 assessing the number of events related to a large displacement, such as the one
725 observed at the *Tio rey* trench. **Figure 7a** is a synthesis of the event chronologies
726 where the time uncertainty (time span) of each event is represented along the X axis.

727 In order to assess a minimum number of PEs derived from the correlation
728 between the different trenches, we first compared the two trenches recording a
729 maximum number of events, i.e. the *Carrascos* and *Gabarrones* trenches. These
730 trenches are located at ca. 500 m from each other so that correlation between the units
731 exposed is easier than between more distant trenches. The correlation of events
732 recorded at these two trenches enables us to infer a minimum of 6 paleoearthquakes:
733 **1)** PE 1 corresponds to event Ca-1, which is not recorded at the *Gabarrones* trench; **2)**
734 PE 2 is event Ca-2, which matches Ga-1; **3)** PE 3 and PE 4 are represented at
735 *Gabarrones* by Ga-2 and Ga-3, respectively. One of these events matches Ca-3 at the
736 *Carrascos* trench; **4)** PE 5 corresponds to events Ca-4 and Ga-4 and, **5)** PE 6
737 corresponds to events Ca-5 and Ga-5.

738 By correlating the time-distribution of these 6 PEs with that of the events at the
739 other trenches, it is possible to refine the age constraints of the PEs. Some events can
740 be correlated in a unique mode. However, others might correspond to several of the
741 PEs identified at *Carrascos* and *Gabarrones*. The analysis of the possible
742 combinations of events allows us to consider three chronologies (known as options 1
743 to 3) as compatible with the event timing determined in this work (**Fig. 7a**). The time
744 constraint resulting from each specific combination of events is specified in brackets
745 next to each PE.

746 In the three options PE1, 5 and 6 are defined in the same way; PE1 (3 - 25 ka)
747 is defined by events Ca-1 and Tr-1; PE5 (135 – 208) is defined by events Ca-4 and Ga-
748 4, and; PE6 (174 – 274 ka) is defined by events Ca-5 and Ga-5. Era-1 matches PE1 but
749 also PE2 in all of the options, but this does not change the time range of the PEs. The
750 same thing happens with Ca-3, which matches PE 3 and PE 4, and with Sa-3, which
751 could represent PE 4, 5 or 6. The multiple event Tr-X could include all the 6 PEs.

752 The three PE chronologies result from a different combination of events in PE
753 2 to 4, and are defined as follows: **Option 1**). In this option PE 2 (21 -51 ka) is defined
754 by Ca-2 and Ga-1; PE 3 (47 - 63 ka) is defined by events, Ga-2 and Sa-1, and; PE 4
755 (59 - 116) is represented by events Ga-3 and Sa-2. **Option 2**). In this option PE 2 (39 -
756 51 ka) is defined by Ca-2, Ga-1 and Sa-1; PE 3 (59 - 116 ka) is defined by events, Ga-
757 2 and Sa-2, and; PE 4 (99 and 116) is represented by events Ga-3 and Sa-3. **Option 3**).
758 In this option, PE 2 (39 - 51 ka) is represented by Ca-2, Ga-1, and Sa-1; PE 3 (46 - 116
759 ka) is only defined by event Ga-2, and; PE 4 (59 and 116) is defined by events Ga-3
760 and Sa-2.

761 Of the three options, option 2 is the one that yields a finer age constraint for
762 two of the PEs, PE 2 and PE 4. This is because in these two PEs events of compatible
763 but very different age constraints are being correlated, i.e. the dated samples used to
764 define the events yield more contrasting ages than in the other options.

765 Apart from these PEs, a more recent PE could have been recorded at the *Tio*
766 *Rey* and *Carrascos-2* trenches, where an apparent rupture of the soil was observed.
767 The interpretation of these ruptures as a very recent rupture, younger than 3 ka
768 (minimum age constraint of PE 1) is not straightforward, and should be borne in mind
769 in future research. As mentioned in section 5, the apparent offset of the soil unit could
770 be the result of an adaptation of the soil to the fault zone, which is harder than the

771 surrounding material at both trenches. Moreover, the displacement could be real but
772 the soil could be an exhumed soil affected by pedogenetic processes.

773 In the case of very recent ruptures, the absence of an associated surface scarp could be
774 attributed to two factors: **a)** the enhanced erosion affecting the surface and/or **b)** the
775 obliteration of the slip by natural erosion or agricultural transformation of the land.

776

777 *Seismogenic segmentation of the Goñar fault strands*

778 The comparison of the event chronologies of the different trenches helped us to better
779 understand the seismogenic behavior of the system during an earthquake.

780 The event chronologies suggest that seismogenic ruptures are able to propagate along
781 all the length of the fault splay, as evidenced by a similar number of events recorded at
782 the opposite trenches, i.e. *Carrascos-1* and *Sardinas* (**Fig. 6** and **Fig 7a**).

783 However, a comparison of the frontal and the inner fault strands shows some
784 differences. The north-westernmost strands (FS1 - *Gabarrones* and FS4 - *Sardinas*) do
785 not seem to have been active during the last two PEs (PE1 and the recent earthquake
786 possibly recorded at *Tio Rey* and *Carrascos-2*). Conversely, the remaining PEs seem
787 to have been recorded at all the fault strands of the Góñar system, which suggests that
788 all the strands could move simultaneously. FS 1 and FS 4 are aligned and could be part
789 of a single fault trace. Since such a fault trace is located in the hinterland of the
790 system, the cessation of its activity during the most recent PEs can be interpreted as
791 the result of a transfer of the activity to the SE in a piggyback manner. Further
792 evidence is warranted for a detailed discussion of this subject.

793

794 *6.2 Correlation of the event chronologies with neighboring paleoseismologic sites*

795 The linkage between the AMF and the Albox fault has been discussed in earlier
796 studies (e.g. Masana et al., 2005; Pedrera et al., 2010), as has the seismogenic
797 segmentation of the AMF (Martínez-Díaz, 1998; Martínez-Díaz et al., 2001, 2003;
798 Masana et al., 2004, 2005; Silva et al., 1997, 2003).

799 The chronology of paleoearthquakes obtained in this work can be compared
800 with that obtained in earlier studies in the area. Since these studies concern trenches
801 with only young units (in contrast to the Góñar trenches) only the chronology of PE1
802 and 2 can be compared.

803

804 *Góñar and Lorca sites*

805 A comparison of the event chronologies of the trenches at the Góñar fault system with
806 those at the SAMF at Lorca (**Fig 7b**) yields the following scenarios: **scenario 1**) the
807 “simultaneous” rupture of the two fault zones during PE1 and PE2, **scenario 2**) the
808 fault ruptures are different in one of the PEs but are the same in the other and **scenario**
809 **3**) none of the PEs corresponds with events at the Lorca sites. In scenario 1, the
810 “simultaneous” rupture could be due to a single event or to two independent events
811 during which one of the fault segments triggered the slip in the other segment. It is not
812 possible to differentiate the single rupture from the triggered rupture by using the
813 available time constraints since a triggering behavior means that such successive
814 events could be separated by minutes or hours.

815 If it were assumed that the simultaneous rupture of the entire Lorca – Góñar
816 system took place (scenarios 1 and 2), the age-range of the events at Góñar would be
817 narrowed because the timing of the events at the Lorca sites (reported in Martínez-
818 Díaz et al., 2003 and Masana et al., 2004) is better constrained. The proximity between
819 the *El Colmenar* and *El Salvador* sites (**Fig. 1b**) allows us to assume the synchronicity

820 of their events (only two paleoearthquakes are identified). The youngest one would be
821 constrained by events Z (*El Colmenar*) and T (*El Saltador*), henceforth event TZ so
822 that it would have occurred between 830 BC and 1750 BC (this is 2.8 and 3.8 ka ago).
823 The oldest one, represented by event X (*El Colmenar*) and event N (*El Saltador*),
824 henceforth event XN, would have occurred between 16.7 and 26.9 ka ago, but
825 probably immediately before 16.7 ka ago (see Masana et al., 2004 for discussions of
826 these time brackets).

827 For **scenario 1** (simultaneous rupture of the two fault zones during the PE 1
828 and PE 2), PE 1 in the Góñar faults would correspond to event TZ, while PE 2 would
829 match event XN. Then, PE 1 would have occurred between 3 and 3.8 ka ago and PE2
830 between 21 and 26.9 ka ago. PE 2 is only compatible with event XN if the wider time-
831 range of the two last events is considered (and not the most probable age immediately
832 before 16.7 ka). This scenario is not compatible with options *b* and *c* of the Góñar
833 chronologies since PE2 has a minimum age of 39 ka in these options (**Fig. 7a**).

834 For **scenario 2** (the fault ruptures are different in one of the PEs but are the
835 same in the other), three combinations are possible. First, PE 2 only matches the oldest
836 events at Lorca with the age constraints are as in scenario 1 but without correlation of
837 PE 1 and event TZ. PE 2 cannot be correlated with event TZ but only with event XN
838 The two other correlations consider that PE 2 is not simultaneous with events at Lorca,
839 but that only PE 1 can be correlated with either the youngest or the oldest event. If PE
840 1 correlates with the oldest event (XN), then its time constraint would be coincident
841 with the time brackets of event XN, 16.7 and 26.9 ka. This range could be narrowed if
842 the most probable age (immediately before 16.7 ka) is considered. If PE 1 is correlated
843 with the youngest event (TZ), then the chronology is as stated for scenario 1 but with
844 no correlation between PE 2 and the events at Lorca.

845 Scenarios 1 and 2 entail a fault rupture greater than 40 km (**Fig. 1b**), which has
846 major implications for the seismic hazard of the region.

847

848 *Góñar and Albox sites*

849 The ages of event X at the Albox fault are compatible with PE 1 and PE 2 at the Góñar
850 trenches (**Fig. 7b**). If it were synchronous with PE1, such an event would have
851 occurred between 3 and 25 ka, whereas if it were synchronous with PE 2, the time
852 constraint would be between 21 and 38.3 ka. The youngest event recorded at the
853 Albox fault (event Y) is a recent event that apparently occurred during historical times
854 though it is not identified in the historical catalog. This event is not identified at any of
855 the other faults (**Fig. 7b**).

856 These faults can move as reverse faults under a compressive regime oriented
857 N-NW. A continuous co-seismic rupture at the Albox and the Góñar faults is difficult
858 to envisage because of the absence of a clear fault trace between them.

859

860 *6.3 Slip rate across the AMF-Góñar fault system*

861 *Individual slip-rates*

862 The vertical slip rates obtained for individual strands range between 0.01 and 0.08
863 mm/a (**Table 4**). For the *Era* trench (FS5), it was possible to obtain the vertical slip for
864 three horizons: the base of C1, C2 and C3 units. To this end, the logged fold geometry
865 was completed in the upthrown block (for C2 and C3) and the downthrown block (for
866 C1, see **Fig. 6g**). The slip rate using the base of C1 (0.02 - 0.04 mm/a) is in agreement
867 with the one obtained for C3, whereas the slip rate derived for the base of C2 (ca. 0.02
868 mm/a) is similar or smaller. This difference could be due to a slowing down of the slip
869 rate during the deposition of C2 or to a decrease in the average sedimentation rate. It

870 should be noted that the fast floods generating units C1-C3 led to a discontinuous
871 sedimentation rate with the result that variations in the slip rates are expected.

872 The strike slip rates of the NAMF and the SAMF were estimated between 0.45
873 and 1.33 mm/a. The average of the minimum strike slip for these faults is 0.51 mm/a.
874 (**Table 4**).

875 For the NAMF, the strike slip rate was obtained by using the deflections of
876 *Bermeja/Yesos* and *Carrascos/Casas* creek (section 4) and a maximum age of 750 ka
877 (end of the Middle Pleistocene), which was considered to be the most suitable estimate
878 for the emplacement of the Present-day drainage.

879 For the SAMF, the strike slip rate was calculated using **a**) the deflections of
880 channels *a* and *b* incised in the alluvial fan G4 (between *Carrascos* and *El Asno*
881 creeks), bearing in mind that the oldest age for the “un-deflected” channel is the age of
882 the alluvial fan, 125-149 ka (**Fig. 2, Fig. 5, Table 2**) and **b**) the ca. 1 km left lateral
883 fault displacement of the Plio-Quaternary strata of La Gata Hills (section 4) for which
884 1.6 M.a. is considered a minimum age.

885 A net slip rate of 0.04 – 0.06 mm/a was obtained for FS1 at *Gabarrones*. It was
886 only possible to obtain the net slip here because of the lack of good kinematic
887 indicators at the other trenches. A net slip of 2.87 - 3.01 m was inferred from a vertical
888 slip of 1.26 - 1.31 m at fault *b* (087°/25°S and 70° W pitch). The net slip rate obtained
889 (0.04 – 0.06 mm/a) is much larger than the vertical (0.02 -0.03 mm/a) and the strike
890 slip rate (0.02 mm/a). The wide range of slip vectors observed in the study area is
891 likely to be the result of the structure formed by fault bounded blocks, which may
892 induce space constrictions on the movements of the blocks. Therefore, it is not
893 recommendable to use the net to dip slip relationship observed at *Gabarrones* to
894 estimate the net slip at the other sites.

895

896 *Summed slip-rates*

897 For the time range between 47 and 63 ka, the sum of the vertical slip rates of the
898 Góñar strands 1, 2 and 3 in the northern area (*Carrascos* and *Gabarrones* sites) varies
899 between 0.04 and 0.07 mm/a, which is lower than the values obtained for the system in
900 the southern sector (*Era* and *Sardinas* sites), 0.07 -0.12 mm/a (**Table 4**). This suggests
901 that a greater accumulated vertical uplift takes place in this area with respect to the
902 northernmost sites. Such an increase in the vertical slip of the system is in agreement
903 with the orientation of the fault traces that are more perpendicular to the NW-SE
904 convergence direction (**Fig. 1a**). The total vertical slip of the AMF-Góñar fault system
905 could double these values should a similar slip rate be attributed to the NAMF and
906 SAMF. Such an assumption yields vertical slip values in the range of 0.16 and 0.22
907 mm/a.

908 The total minimum strike slip rate of the AMF-Góñar system was estimated
909 between 0.95 and 1.37 mm/a. This value was obtained by adding the rates of the
910 NAMF and the SAMF to the sum of rates in the Góñar faults (**Table 4**). The latter
911 value is close to 0.04 mm/a, twice the strike slip rate at *Gabarrones*, since the Góñar
912 system in *Gabarrones* transect is made up of two strands. The slip rates considered are
913 obtained using markers of very different ages, which introduces considerable
914 uncertainty. Such a total minimum value would be lower if the NAMF were not active
915 during the late Pleistocene-Holocene.

916 A further estimation of the summed slip rate was done by extrapolating the net
917 slip rate obtained at *Gabarrones* (0.04 – 0.06 mm/a) to the remaining fault strands.
918 This led to a total net slip rate of the AMF-Góñar fault system at *Gabarrones* transect
919 between 0.16 – 0.24 mm/a, for the system here is made up of at least four fault strands.

920 The large difference between the summed slip rates obtained by these different
921 approaches shows that these estimations have large uncertainties.

922

923 *Comparison of slip-rates with neighboring fault segments*

924 The summed vertical slip rates of the fault strands in the AMF-Góñar system (0.16 –
925 0.22 mm/a since 47 – 63 ka) are considerably greater than the values observed at the
926 Albox fault (0.01 and 0.04 mm/a, Masana et al., 2005) and are comparable or smaller
927 than those observed at the central AMF at Lorca. There, Masana et al. (2004) have
928 reported vertical slip rates between 0.04 and 0.35 mm/a on the SAMF strand for the
929 last 30 ka (**Table 1**). This could represent a half of the total vertical slip, which would
930 range between 0.08 – 0.70 mm/a if the SAMF rate is extrapolated to the NAMF (**Fig.**
931 **1b**). A decrease in the vertical slip from the central parts of the AMF (at Lorca)
932 towards the tips of the system (at Góñar) is suggested. A similar decrease is observed
933 in the net slip rates; At the SAMF in the Lorca trenches, the net slip rates for the last
934 30 ka range between 0.53 and 0.66 mm/a (Masana et al. 2004), whereas at the
935 *Gabarrones* transect, the rates vary between 0.16 – 0.24 mm/a, assuming the
936 deformation of the system is equally partitioned among four fault strands. This
937 decrease of the vertical and net slip rates is consistent with the expected variations in
938 slip from the center to the tips of the faults and would be compatible with the two sites
939 being part of a single fault segment.

940 The strike slip rates obtained at Lorca using the pitch of slickenlines on the
941 SAMF are 0.06 – 0.53 mm/a. These values are comparable or smaller than those
942 obtained for the SAMF and the NAMF at Góñar (between 0.45 and 1.33 mm/a). If
943 smaller, the difference could be indicative of **1**) a decrease in the activity of the fault
944 with time, since the age of the markers used at Lorca (30 ka) is much younger than the

945 age used for Góñar (100-175 ka and 750 ka) or **2**) as an overestimation of the slip rate
946 at Góñar related to an underestimation of the age considered for the calculations. This
947 latter possibility would invalidate the unusually large strike-slip rates for Góñar
948 estimated above so that the decrease in the vertical slip rate from the central to the
949 southern tip of the AMF would not be contradicted by the strike-slip rates. Smaller slip
950 rates would also be more consistent with the recurrence period obtained below.

951

952 *6.4 Paleoseismic Parameters*

953 *Slip per event*

954 The NAMF, the SAMF and the Góñar fault system form a horse-tail structure as
955 suggested by the fault pattern (in map view) and the fault geometry with the result that
956 all the faults could be connected at depth. This implies that the different strands could
957 all move simultaneously during an earthquake. In such a case, the slip per event
958 observed at the trenches at the Góñar faults is a minimum value that could only
959 represent one fourth of the total slip (or even less if the slip at the boundary faults is
960 greater). The only trench for which the net slip was calculated is *Gabarrones* (event
961 Ga-2). The net slip recorded, 1.15 ± 0.25 m, can be taken as a minimum slip per event
962 associated with the system. A similar slip in the 4 strands of the system at the
963 *Gabarrones* transect would mean a slip per event between 3.6 and 5.6 m. In
964 accordance with empirical relations proposed by Stirling (2002) such single event
965 displacements are linked to faults that are about 400 km long whereas the AMF does
966 not exceed 150 km in length. This suggests that **1**) the slip is distributed in an irregular
967 manner among the 4 strands of the system, or **2**) the 1.15 ± 0.25 m slip corresponds to
968 more than one earthquake or that **3**) the faults do not move simultaneously.

969 Another way of estimating the minimum slip per event is to consider the
970 accumulated slip recorded at some of the trenches. For instance, at *Tio Rey*, the 6 PEs
971 could have been recorded in the large displacement of unit J by fault *b* (6.72 ± 0.74 m
972 along the dip) as well as in the displacement along the other faults at this trench (**Fig.**
973 **6e**). This yields a slip along dip per event of 1.12 ± 0.12 m, which could be smaller if
974 the number of paleoearthquakes represented were greater. In the *Era* trench, the
975 vertical offset of the base of unit C1, 4.31 – 5.05 m probably reflects the displacement
976 of 4 to 5 earthquakes. According to the event chronologies (**Fig. 7a**), this number of
977 earthquakes is the minimum number that occurred after the deposition of unit C1
978 (dated as 124 – 149 ka old). These values yielded maximum vertical-slip per events
979 between 0.86 and 1.26 m at FS5, which is over the range of the average slip per event
980 observed at the paleo-seismological sites in the region (**Table 1**).

981 The aforementioned estimates yielded vertical slips per event in the range of
982 1.7 – 2.8 m (twice the range of 0.86 - 1.4 m calculated for a single strand).

983

984 *Maximum expected earthquake magnitude*

985 To estimate the maximum expected magnitude associated with the seismic rupture of
986 the AMF-Góñar system, we used the length of the system rather than the slip per event
987 observed at the trenches. The reason for this was twofold: **a**) the large uncertainty
988 associated with the values of slip per event observed, which in most cases did not
989 correspond to the net slip, and **b**) the fact that the slip is distributed among several
990 fault strands so that the real value cannot be well constrained.

991 The length of the traces of the Góñar fault system is ca. 6 km, which is a minimum
992 estimate of the length of the AMF southern splay (see section 4). The surface rupture
993 of a 6 km fault can be related to an earthquake magnitude of $M_w = 5.9$ by using the

994 empirical relationships that Berryman et al. (2002) proposed for strike slip and reverse
995 faults in New Zealand. A similar value, $M_w = 6.0$, is obtained through the general
996 equations of Wells and Coppersmith (1994). These magnitudes are slightly greater
997 than the $M_w = 5.6$ magnitude obtained using the Hanks and Bakun (2002)
998 relationships for strike slip earthquakes in global plate boundaries.

999 The co-seismic rupture of the entire Góñar-Lorca fault segment (40 km) should
1000 also be considered. Given the lack of paleoseismical studies in the area between these
1001 localities, the possible propagation of a seismogenic rupture through the 40 km fault
1002 trace cannot be ruled out. Employing the aforementioned empirical relationships, such
1003 a fault rupture can be related to earthquakes with $M_w = 7.0$ (equations in Berryman et
1004 al., 2002), $M_w = 6.9$ (equation in Wells and Coppersmith, 1994) and $M_w = 6.7$
1005 (equations in Hanks and Bakun, 2002).

1006 An alternative “intermediate” scenario is the co-seismic rupture from Góñar to
1007 the area immediately north of Puerto Lumbreras (Fig. 1b), where a step-over in the
1008 fault trace could act as a barrier for the propagation of the fault. In this case, the fault
1009 length would be ca. 15 km, which can be related to earthquake magnitudes of $M_w =$
1010 6.1 – 6.4 according to the three aforementioned empirical relationships.

1011 For the calculations above, we used a rupture width of 12 km, which is the
1012 most accepted value for the seismogenic crust in the area (García-Mayordomo, 2005).

1013 The 6 km rupture length is the less probable among all the options discussed. It
1014 would be unusually small length for a seismogenic rupture in accordance with the
1015 values commonly observed (e.g., Wells and Coppersmith, 1994; Gasperini et al., 1999;
1016 Stirling et al., 2002) at the time that it would be related to average co-seismic
1017 displacements much smaller (ca. 0.18 m according to equations in Wells and

1018 Coppersmith, 1994) than the expected for the Góñar-system (more than 0.86 – 1.26
1019 m).

1020 These estimated magnitudes pose a significant risk in this area, where most of
1021 the towns are built on top of alluvial sediments that could trigger amplification of the
1022 seismic waves and liquefaction. This was shown to be crucial during the Lorca
1023 earthquake (11/05/2011, $M_w = 5.1$), which caused peak ground accelerations in the
1024 order of 0.36 g (IGN, 2011), three times greater than the value assigned to the area in
1025 the Spanish seismo-resistant construction code (NCSR-02, 2002).

1026

1027 *Recurrence period*

1028 A preliminary estimate of the maximum value of the mean recurrence period of
1029 the Góñar fault system can be obtained by considering the three options for the
1030 paleoearthquake chronology discussed in the foregoing section. In the three options,
1031 the four latest paleoearthquakes occurred within a maximum period of 108-116 ka.
1032 Assuming a periodic behavior for the fault ruptures, we obtained an average time of 27
1033 - 29 ka between two successive earthquakes. However, in options 1 and 3, PE 4 could
1034 have occurred 59 - 63 ka ago, which yields a recurrence period of 15 - 16 ka. When
1035 considering the last 6 PEs, the maximum recurrence period increases to 29 - 47 ka. If
1036 only the last 5 PEs are considered, the recurrence ranges from 27 to 42 ka.

1037 Summarizing, the maximum recurrence period yielded ranges between 15 and
1038 29 ka for the last 108-116 ka. The minimum value is similar to the recurrence interval
1039 obtained at the Lorca trenches (ca.14 ka, Masana et al., 2004) whereas the maximum
1040 value approximately doubles it .The 15 - 29 ka range for the recurrence interval is, at
1041 any case, larger than the ca. 8 ka recurrence interval obtained from a maximum total
1042 slip rate of 0.24 mm/a and a minimum of ca. 2 m of summed slip per events deduced

1043 for the system. This latter value is a robust estimation of the minimum summed slip as
1044 observed in the trenches. Therefore, such a discrepancy could be due to an
1045 underestimation of the number of paleoearthquakes, which in any case is considered as
1046 a minimum, and/or to an overestimation of the total slip rate of the system.

1047 The rough estimate of the recurrence period made here concerns the large
1048 uncertainties associated with the time-constraint of the events, i.e. the result of the
1049 large time difference between the units bracketing the events. Since this is related to
1050 the discontinuous sedimentological record that characterizes the study area, this aspect
1051 constitutes a major limitation. A better estimate of the real recurrence period in the
1052 area, however, could be obtained in with paleoseismic data from other sites along the
1053 studied fault strands and from the NAMF and SAMF strands.

1054

1055 *6.5 Insights into the geodynamics of the AMF-Góñar system*

1056 The structure observed at the southern tip of the AMF, which is made up of a
1057 splay of synthetic and antithetic faults, can be explained by two models: **a)** the
1058 structure is inherited from the earlier extensional tectonic regime. Similar splay
1059 geometries have been observed at the tip of extensional systems within the continental
1060 crust by Bahat (1991) and Suter et al. (2001) among others; **b)** the structure
1061 corresponds to a horse-tail termination generated by the growth of the AMF as a strike
1062 slip structure, active since the latest Miocene. Whichever its origin, we documented a
1063 significant reverse slip in this part of the AMF, where the structure changes its
1064 orientation. The strike-slip component of the inner faults of the splay (the Góñar
1065 faults) is minor compared to the reverse slip.

1066 The southwestern tip of the AMF seems to behave like a compressional bend in
1067 which the strike of the faults undergoes a clockwise rotation that favors a larger
1068 shortening component under the NNW-SSE S_{hmax} direction. A similar geometry is

1069 observed in the central part of the AMF in the Lorca-Totana segment (Martínez-Díaz,
1070 1998; Martínez-Díaz et al. 2003; Masana et al., 2004) and in the neighboring
1071 northeastern tip of the Carrascoy fault (Fig. 1) as described by García-Mayordomo and
1072 Martínez-Díaz (2006). The NNW-SSE S_{hmax} differs from the interplate NW-SE
1073 convergence azimuth proposed by Argus et al. (1989) for this interplate transect. This
1074 could be due to an inland rotation of the convergence direction or to local variations in
1075 the maximum horizontal compression. The latter situation is expected when the
1076 interplate deformation is accommodated through structures that are inherited from
1077 previous tectonic regimes and that show a variety of orientations.

1078

1079 **7. Conclusions**

1080 In this study, we present a ca. 300 ka long paleoseismic chronology of a slow
1081 moving fault zone, the southern tip of the AMF. This is one of the longest
1082 paleoseismic records obtained to date. Since the slow-moving faults are characterized
1083 by long recurrence intervals (greater than tens of ka), the time observation window
1084 required to observe several successive earthquakes is in the order of hundreds of ka.

1085 A number of factors contributed to the study of this long paleoseismic history:

1086 **a)** The presence of a splay structure. This structure showed simultaneous rupture along
1087 its fault strands, which provided us with more opportunities to refine the time
1088 constraint of the recorded paleoearthquakes. This could not have been done in a
1089 single-structure or at single paleoseismic site; **b)** The possibility of dating units as old
1090 as 325 ka by a new luminescence dating protocol developed by Sohbati et al. (2011).
1091 This new technique, which measures the luminescence radiation on K-feldspar
1092 grains, extends the range for numerical dating of Quaternary sediments, usually
1093 limited to less than 100 ka, and **c)** The alluvial sedimentary environment with a
1094 condensed (although not continuous) sedimentation. Such a sedimentological setting

1095 combined with a faulting style consisting of oblique-reverse faulting and fault-
1096 propagation folding enabled the observation of different alluvial fan phases in
1097 relatively shallow trenches (of less than 3 m depth).

1098 We documented a fault zone (1.5 km wide and minimum length of 6 km long)
1099 made up of 4 to 5 fault strands. The deformation has been partitioned into the different
1100 strands. The overall structure is characterized by 1) oblique slip with reverse and left
1101 lateral movement, 2) slip rates between 0.03 and 0.12 mm/a in the internal structures
1102 (Góñar faults), and between 0.16 and 0.24 mm/ for the AMF-Góñar system, which
1103 includes the ANMF and the SAMF. . The activity along the fault system has given rise
1104 to a compressional bend between the uplifted *Las Estancias* range and the *Huerca-*
1105 *Overa* and *Guadalentin* depressions. This deformation forms a smaller secondary
1106 range front that emerges in the *Guadalentin* basin, conditioning the draining network.
1107 A possible foreland migration of the deformation is observed.

1108 The paleoseismologic data provided new insights into the segmentation of the
1109 AMF. The integrated analysis of the event chronologies at six different trenches
1110 yielded a minimum of 6 paleoearthquakes during the last 174 – 274 ka, with a
1111 maximum recurrence interval between 15 and 29 ka for the last 59 - 116 ka.
1112 Correlation of the paleoearthquakes at the southwestern tip of the AMF with those
1113 previously observed in the central part (Lorca) and at the neighboring Albox fault
1114 indicates a feasible synchronicity of the fault ruptures, which suggests that a maximum
1115 $M_w = 7$ earthquake could occur in the area. These results should be considered in the
1116 seismic hazard assessment of the area. This is of paramount importance in this region
1117 of the Iberian Peninsula, where a movement in the central segment of the AMF
1118 recently produced a shallow $M_w = 5.1$ earthquake (5.11.5.2011), leaving thousands of
1119 people homeless and causing considerable economic loss.

1120

1121 **Acknowledgements**

1122 This work was founded by the Spanish Ministerio de Educación y Ciencia through the
1123 EVENT (CGL2006-12861-C02-01/BTE) and the SHAKE (CGL2011-30005-C02-
1124 01/BTE) projects, the Consolider-Ingenio 2010 program, under CSD2006-0004 "Topo-
1125 Iberia", and in part by the project PTDC/CTE-GIN/66283/2006 (approved by the FCT
1126 and co-founded by the FEDER). We would like to express our gratitude to Y. Vázquez,
1127 R. Roper, A. Caro and O. Romero for their field assistance and to the R. Ayala family,
1128 to David and Dora and to M. Peralta of Góñar. We are very grateful to A.Soler (Dept.
1129 Desertificación y Geoecología, CSIC-España) and to P. Ruano (Dep. Geología, Univ.
1130 Granada) for their helpful discussions in the field. The TL dating was carried out by
1131 *Quaternary TL Surveys* (Nottingham, UK) and the OSL dating at the Earth Sciences
1132 Dep – Universidade de Coimbra (sample-treatment) and at the Nordic Laboratory for
1133 Luminescence Dating of the Aarhus University (OSL measurements). The final version
1134 of the paper improved considerably thanks to the reviews and suggestions made by Pilar
1135 Villamor and John Wakabayashi.

1136

1137 **References**

1138 Argus, D. F., R. G. Gordon, C. DeMets, and S. Stein (1989), Closure of the Africa-
1139 Eurasia-North American plate motion circuit and tectonics of the Gloria Fault, J.
1140 Geophys. Res., 94, 5585– 5602.

1141 Bahat, D., 1991. Certain mechanical aspects in comparative continental rifting with
1142 special reference to the Baikal rift. Geol., Mag., 118, 271-280.

1143 Banda, E., Ansorge, J., 1980. Crustal structure under the central and eastern part of the
1144 Betic Cordillera. Geophys. J. Roy. Astr. Soc 63, 515–532.

1145 Bardají, T., 1999. Evolución Geodinámica de la Cuencas neógenas del litoral de Murcia
1146 y Almería durante el Cuaternario. PhD Thesis, UCM, Madrid, Spain. 457 pp.

1147 Berryman, K., Webb, T., Hill, N., Stirling, M., Rhoades, D., Beavan, J., and Darby, D.,
1148 2002. Seismic loads on dams, Waitaki system. Earthquake source characterisation.
1149 Main report, GNS client report 2001/129.

1150 Bousquet, J.C. and Montenat, C., 1974. Presence de décrochements NE-SW plio-
1151 quaternaires dans les Cordillères Bétiques Orientales (Espagne). Extension et
1152 signification général, C.R. Acad. Sci. Paris, 278, 2617-2620.

1153 Bousquet, J.C., 1979. Quaternary strike-slip faults in southeastern Spain.
1154 Tectonophysics, 277–286.

1155 Briend, M., 1981. Evolution morpho-tectonique du basin neogene de Huércal Overa
1156 (Cordilleres Béticas orientales-Espagne). Documents et travaux, IGAL 4, 208 pp.

1157 Buylaert J.P., Murray A.S., Thomsen K.J. and Jain M., 2009. Testing the potential of an
1158 elevated temperature IRSL signal from K-feldspar. Radiation Measurements 44, 560-
1159 565.

1160 De Mets, Ch., Gordon, R.G., Argus, D.F., and Stein, S., 1994. Effect of recent revisions
1161 to the geomagnetic reversal time scale on estimate of current late motions. Geophys.
1162 Res. Lett. 21, 2191–2194.

1163 Garcia-Mayordomo, J. (2005). Caracterización y Análisis de la Peligrosidad Sísmica en
1164 el Sureste de España. [PhD thesis]: Universidad Complutense de Madrid, 373 pp.

1165 García-Mayordomo, J., and Martínez Díaz, J., 2006. Caracterización sísmica del
1166 Anticlinorio del Bajo Segura (Alicante): Fallas del Bajo Segura, Torrevieja y San
1167 Miguel de Salinas. Geogaceta, 40, 19-22

- 1168 García-Meléndez, E., 2000. Geomorfología y Neotectónica del Cuaternario de la cuenca
1169 de Huércal-Overa y corredor del Almanzora. Análisis y Cartografía mediante
1170 Teledetección y SIG. [Ph.D. thesis]: Universidad de Salamanca, 528 pp.
- 1171 García-Meléndez, E., Goy, J.L., and Zazo, C., 2003. Neotectonica and Plio-Quaternary
1172 landscape development within the eastern Huércal-Overa Basin (Betic Cordilleras,
1173 southeastern Spain). *Geomorphology* 50, 111–133.
- 1174 García-Meléndez, E., Goy, J.L., and Zazo, C., 2004. Quaternary tectonic activity in the
1175 Huércal-Overa Basin (Almería Southeast Spain): deformations associated with the
1176 Albox fault. *Geogaceta* 36, 63–66.
- 1177 Gasperini, P., Bernardini, F., Valensise, G. and Boschi, E., 1999. Defining Seismogenic
1178 Sources from Historical earthquake Felt Reports. *Bulletin of the Seismological*
1179 *Society of America*, 89(1), 94-110.
- 1180 Gauyau, F., Bayer, R., Bousquet, J.C., Lachaud, J.C., Lesquer, A., and Montenat, C.,
1181 1977. Le prolongement de l'accident d'Alhama de Murcia entre Murcia et Alicante
1182 (Espagne Résultats d'une étude géophysique méridionale). *Bull. Soc. Géol. France*,
1183 *Série 7* 19, 623–629.
- 1184 Hanks, T.C. and Bakun, W.H., 2002. A bilinear source-scaling model for M-logA
1185 observations of continental earthquakes. *Bulletin of the Seismological Society of*
1186 *America* 92, 1841 – 1846.
- 1187 IGN, 2010. Servicio de información sísmica del Instituto Geográfico Nacional
1188 de España (<http://www.ign.es/ign/es/IGN/SisIndice.jsp>).
- 1189 IGN, 2010. Serie sísmica del terremoto de Lorca, Murcia (11/05/2011).
1190 (<http://www.ign.es/ign/resources/sismologia/Lorca.pdf>)
- 1191 McCalpin, J.P., 1996. *Paleoseismology*. Academic Press, San Diego, 588 pp.

1192 McClusky, S.R., Reilinger, S., Mahmoud, D., Ben Sari, and Tealeb, A., 2003. GPS
1193 constraints on Africa (Nubia) and Arabia plate motions. *Geophys. J. Int.* 155, 126–
1194 138.

1195 Martínez-Díaz, J.J., 1998. Neotectónica y tectónica activa del sector Centro-occidental
1196 de la región de Murcia y sur de Almería (Cordillera Bética- España). [Ph.D. thesis]:
1197 Universidad Complutense de Madrid, 466 pp.

1198 Martínez-Díaz, J.J., Masana, E., Hernández-Enrile, J.L., Santanach, P., 2001. Evidence
1199 for coseismic events of recurrent prehistoric deformation along the Alhama de
1200 Murcia fault, southeastern Spain. *Acta Geológica Hispánica* 36, 315–327.

1201 Martínez-Díaz, J.J., Masana, E., Hernández-Enrile, J.L., and Santanach, P., 2003.
1202 Effects of repeated paleoearthquakes on the Alhama de Murcia Fault (Betic
1203 Cordillera, Spain) on the Quaternary evolution of an alluvial fan system. *Ann.*
1204 *Geophys.* 46 (5), 775–792.

1205 Martínez-Díaz, J.J., Capote, R., Tsige, M., Villamor, P., Martín-González, F., and
1206 Insua-Arevalo, J.M., 2006 Seismic triggering in a stable continental area : the Lugo
1207 1995-1997 seismic sequences (NW Spain). *Journal of Geodynamics*, 41(4): 440-449.

1208 Martínez-Díaz, J., Masana, E., and Ortuño, M., 2010. Implications of the structure of
1209 the Alhama de Murcia Fault on its paleoseismological analysis. Extended abstracts of
1210 the 1st Iberian meeting on active faults and paleoseismology, Sigüenza (Guadalajara,
1211 Spain), 97 -100..

1212 Masana, E., Martínez-Díaz, J.J., Hernández-Enrile, J.L., and Santanach, P., 2004. The
1213 Alhama de Murcia fault (SE Spain), a seismogenic fault in a diffuse plate boundary.
1214 Seismotectonic implications for the Ibero-Magrebian region. *J. Geophys. Res.* 109,
1215 1–17.

1216 Masana, E., Pallàs, R., Perea, H., Ortuño, M., Martínez-Díaz, J.J., García-Meléndez, E.,
1217 and Santanach, P., 2005. Large Holocene morphogenic earthquakes along the Albox
1218 fault, Betic Cordillera, Spain. *J. Geodynamics* 40, 119–133.
1219 doi:10.1016/j.jog.2005.07.002.

1220 Meijninger, B.M.L., 2006. Late-orogenic extension and strike-slip deformation in the
1221 Neogene of southeastern Spain. [Ph.D. thesis]: Universiteit Utrecht. *Geologica*
1222 *Ultraiectina*, 179 pp.

1223 Montenat, C., 1973. Les formations néogènes du levant espagnol. [Ph.D. thesis]:, Orsay,
1224 University of Paris, 1170 p.

1225 Montenat, C., 1996. The Betic Neogene basins: introduction. In: P.F. Friend and C.
1226 Dabrio (Eds.), *Tertiary Basins of Spain*, Cambridge University Press, pp 321 – 322.

1227 Montenat C., and Ott d’Estevou, P., 1996. Late Neogene basins evolving in the Eastern
1228 Betic transcurrent fault zone: an illustrated review, In: P.F. Friend and C. Dabrio
1229 (Eds.), *Tertiary Basins of Spain*, Cambridge University Press, pp 372 – 386.

1230 NCSR-02, 2002, Norma de construcción sismorresistente NCSE-02. Parte General y
1231 Edificación. Anexo al Real decreto 997/2002 de 27 de septiembre. BOE núm. 244.
1232 Sábado 11 de octubre de 2002. pp. 35898-35967.

1233 Pedrera, A., Galindo-Zaldivar, J., Tello, A., and Marin-Lechado, C., 2010. Intramontane
1234 basin development related to contractional and extensional structure interaction at the
1235 termination of a major sinistral fault: The Huercal-Overa Basin (Eastern Betic
1236 Cordillera), *Journal of Geodynamics*, Volume 49, Issue 5, 271-286, doi:
1237 10.1016/j.jog.2010.01.008.

1238 Rodríguez-Fernández, J., and Sanz de Galdeano, C., 1992. Onshore neogene
1239 stratigraphy in the north of the Alboran sea (Betic Internal Zones): Paleogeographic

1240 implications. In: A. Madonado (Ed.), The Alboran Sea. *Geo-Mar.Lett.* 12 (2/3), 123-
1241 128.

1242 Sanz de Galdeano, C., 1990. Geologic evolution of the Betic cordilleras in the Western
1243 Mediterranean, Miocene to present. *Tectonophysics*, 172: 107-109.

1244 Sanz de Galdeano, C., and Vera, J.A., 1992. Stratigraphic record and
1245 palaeogeographical context of the Neogene basins in the Betic Cordillera, Spain.
1246 *Basin Research*, 4: 21-36. doi:10.1111/j.1365-2117.1992.tb00040.x

1247 Silva, P., 1994. Evolución geodinámica de la Depresión del Guadalentín desde Mioceno
1248 Superior hasta la actualidad: Neotectónica y Geomorfología, Ph.D. Thesis,
1249 Universidad Complutense de Madrid, 642 pp.

1250 Silva, P., Goy, J.L., and Zazo, C., 1992 a. Características estructurales y geométricas de
1251 la falla de desgarre de Lorca-Alhama. *Geogaceta*, 12: 7-10.

1252 Silva, P., Goy, J.L., and Zazo, C., 1992 b. Discordancias progresivas y expresión
1253 geomorfológica de los abanicos aluviales cuaternarios de la de presión tectónica del
1254 Guadalentín. *Geogaceta* 11: 67-70.

1255 Silva, P.G., Goy, J.L., Somoza, L., Zazo, C., and Bardají, T., 1993. Landscape response
1256 to strike-slip faulting linked to collisional settings: Quaternary tectonics and basin
1257 formation in the Eastern Betics, southeast Spain. *Tectonophysics* 224, 289–303.

1258 Silva, P.G., Goy, J.L., Zazo, C., Lario, J., and Bardají, T., 1997. Paleoseismic
1259 indications along “aseismic” fault segments in the Guadalentín Depression (SE
1260 Spain). *J. Geodyn.* 24, 105– 115.

1261 Silva, P.G., Goy, J.L., Zazo, C., and Bardají, T., 2003. Fault-generated mountain fronts
1262 in southeast Spain: geomorphologic assessment of tectonic and seismic activity.
1263 *Geomorphology* 50, 203–225.

- 1264 Sohbaty, R., Murray, A. S., Buylaert, J.-P., Ortuño, M., Cunha, P. P., and Masana, E.
1265 2011. Luminescence dating of Pleistocene alluvial sediments affected by the Alhama
1266 de Murcia fault (eastern Betics, Spain) – a comparison between OSL, IRSL and post-
1267 IR IRSL ages. *Boreas*, DOI 10.1111/j.1502-3885.2011.00230.x
- 1268 Soler, R., Masana, E., and Santanach, P., 2003. Evidencias geomorfológicas y
1269 estructurales del levantamiento tectónico reciente en la terminación sudoccidental de
1270 la falla de Alhama de Murcia (Cordillera Bética Oriental). *Revista de la Sociedad*
1271 *Geológica de España* 16 (3/4), 123–133.
- 1272 Suter, M., O. Quintero, and Johnson, C. A., 1992. Active faults and state of stress in the
1273 central part of the trans-Mexican volcanic belt 1. The Venta del Bravo Fault. *Journal*
1274 *of Geophysical Research*, 97, p. 11983–11994.
- 1275 Stirling, M., Rhoades, D., and Berryman, K., 2002. Comparison of Earthquake Scaling
1276 Relations Derived from Data of the Instrumental and Preinstrumental Era. *Bulletin of*
1277 *the Seismological Society of America*, 92 (2), 812-830.
- 1278 Thomsen K.J., Murray A.S., Jain M., and Bøtter-Jensen L., 2008. Laboratory fading
1279 rates of various luminescence signals from feldspar-rich sediment extracts. *Radiation*
1280 *Measurements* **43**, 1474-148
- 1281 Voermans, F.M., Geel, T., and Baena, J., 1978. Mapa Geológico de España 1:50.000,
1282 Hoja Velez-Rubio (nº 974). Instituto Geológico y Minero de España.
- 1283 Wells, D.L., and Coppersmith, K.J., 1994. New empirical relationships among
1284 magnitude, rupture length, rupture area and surface displacement. *Bull. Seismol. Soc.*
1285 *A* 84, 974–1002.

1286

1287 **Figure captions**

1288 **Figure 1. a)** Location of the study area within the Betic-Rif cordillera (in the lower

1289 left corner). The white arrow at the lower part of the figure represents the
1290 convergence rate between the Iberian and African plates. The faults marked in
1291 red constitute the Eastern Betics Shear Zone. CRF, Crevillente fault, BSF, Bajo
1292 Segura fault; SMF, San Miguel fault; CF, Carrascoy fault; AMF, Alhama de
1293 Murcia fault; AF, Albox fault; PF, Palomares fault; CBF, Carboneras fault;
1294 HOB, Huercal-Overa Basin; LB, Lorca basin; GDD; Guadalentín depression;
1295 GD, Garita del Diablo. The plate convergence slip vector is indicated by a white
1296 arrow. **b)** Seismicity of the historical catalogue (IGN, 2010) is projected over a
1297 shaded relief map. Note the gap in instrumental-historical seismicity for the
1298 AMF southwestern tip. Previous paleoseismological sites in the area are
1299 indicated: 1, *El Ruchete-Urcal*; 2, *Aljibejo* and *Escarihuela*; 3, *La Carraclaca*; 4;
1300 *El Saltador- El Colmenar*. Other localities: PB, Pulpí basin, TR, La Tercia
1301 range.

1302 **Figure 2. a).** Quaternary morpho-structural map of the study area. The major
1303 neotectonic features are shown together with the geomorphological elements
1304 relevant to this study. Location of the excavated trenches is designated by a
1305 black rectangle and location of other sites of interest, with a star symbol. NAMF,
1306 North Alhama de Murcia fault; SAMF, South Alhama de Murcia fault; S, fault
1307 strand; cr, creek. **b).** Sketch of the displacement of *Bermeja* and *Casas* creeks
1308 produced by the NAMF.

1309 **Figure 3. a)** Structural sketch of the Góñar structure along a NW-SE transect. Data
1310 come from field observations and subsurface information. Secondary faulting
1311 and folding is not included for simplicity. **b)** Sketch of the Góñar structure with
1312 location of the four strands (FFS1 to FFS4) and trenches (black rectangles).

1313 **Figure 4.** General view and detail of deformation observed at several natural and

1314 artificial outcrops in the study area. **a)** *Carrascos-1* trench; **b)** View of the Góñar
1315 fault strand 2 with a sketch of its associated drag fold; **c)** View of the lowlands
1316 associated with the Góñar anticline. The La Gata hills correspond to the SE limb
1317 of this anticline; **d)** View of the Plio-Quaternary strata of the NW limb of the
1318 Góñar anticline at site 2; **e)** *Era* trench; **f)** Present-day soil rupture at the *Tio Rey*
1319 trench; **g)** Colluvial wedges identified at the *Carrascos-1* trench; **h)** Góñar fault
1320 strand 1 displacing Neogene conglomerates next to the *Gabarrones* site; **i)**
1321 Reverse faulting of the beds of the G-4 alluvial phase at site 4; **j)** Fault plane
1322 with slickenlines at the *Gabarrones* trench; **k)** Fault plane of the SAMF at site 3.
1323 A pen is used for scale.

1324 **Figure 5.** Orthophotograph obtained from the 1956 aerial photograph of the area
1325 (scale 1:30000). The horizontal displacement of incipient gullies incised in
1326 alluvial fan G4 is 127 ± 6 m and 77 ± 10 m. The straightening of the main river
1327 channel has left an abandoned channel at the southernmost creek. The
1328 northernmost channel shows a twisted path with two 90° turns.

1329 **Figure 6.** Logs of the six trenches analyzed in this work. See Figure X for location.
1330 Thermoluminescence and K-feldspar optical luminescence ages of the samples
1331 detailed in Table 2 are shown. In the log of Tio Rey trench (e), inset shows a
1332 microtopographic profile perpendicular to the fault trace and including the trench
1333 position.

1334 **Figure 7.** a) Age constraint of the paleoearthquakes in the Góñar area. The bracketing
1335 units are included. In the age axis, the rhombus symbols represent a recurrence
1336 of 25 ka (black) and 20 ka (gray). b) Synthesis of the events observed in the
1337 Góñar area and those deduced in the Lorca-Totana segment of the AMF and in
1338 the Albox fault.

Figure1

[Click here to download Figure: Fig1.pdf](#)

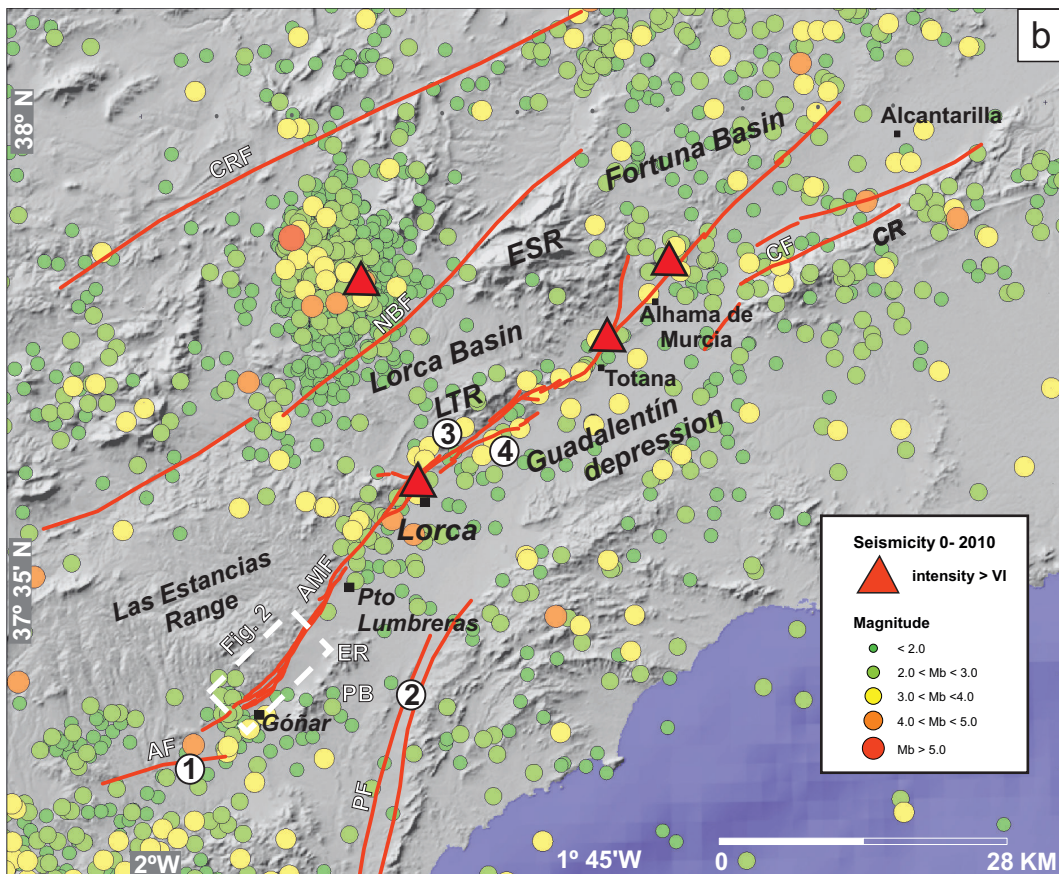
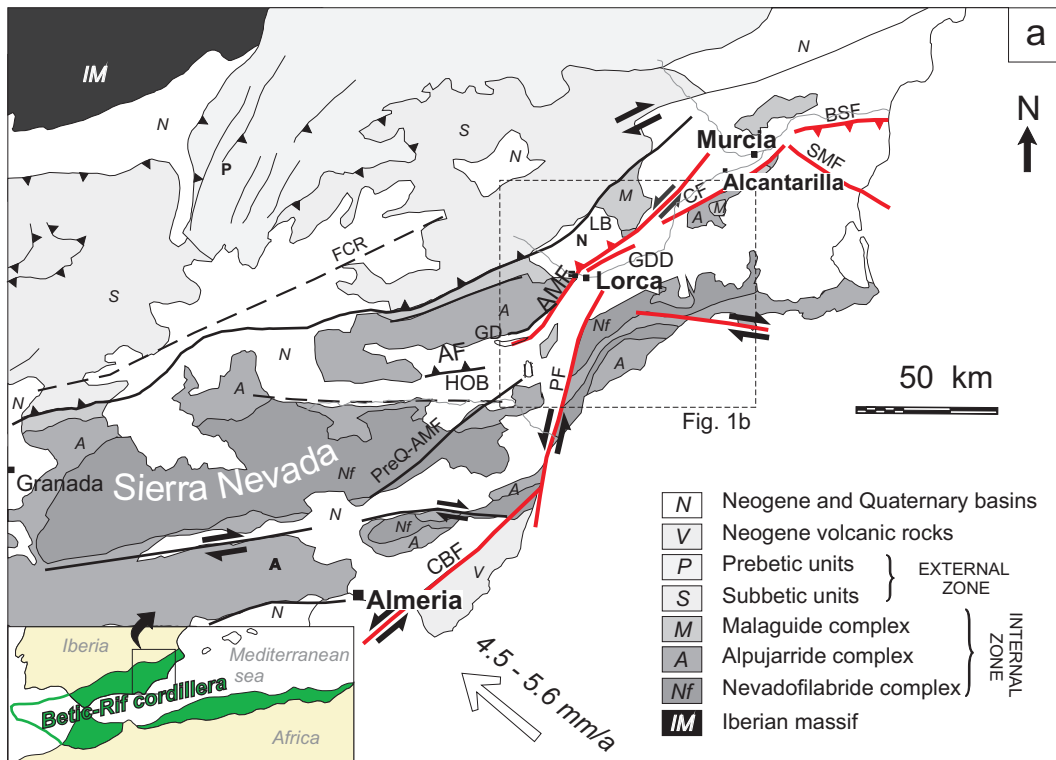


Figure 2

[Click here to download Figure: Fig2.pdf](#)

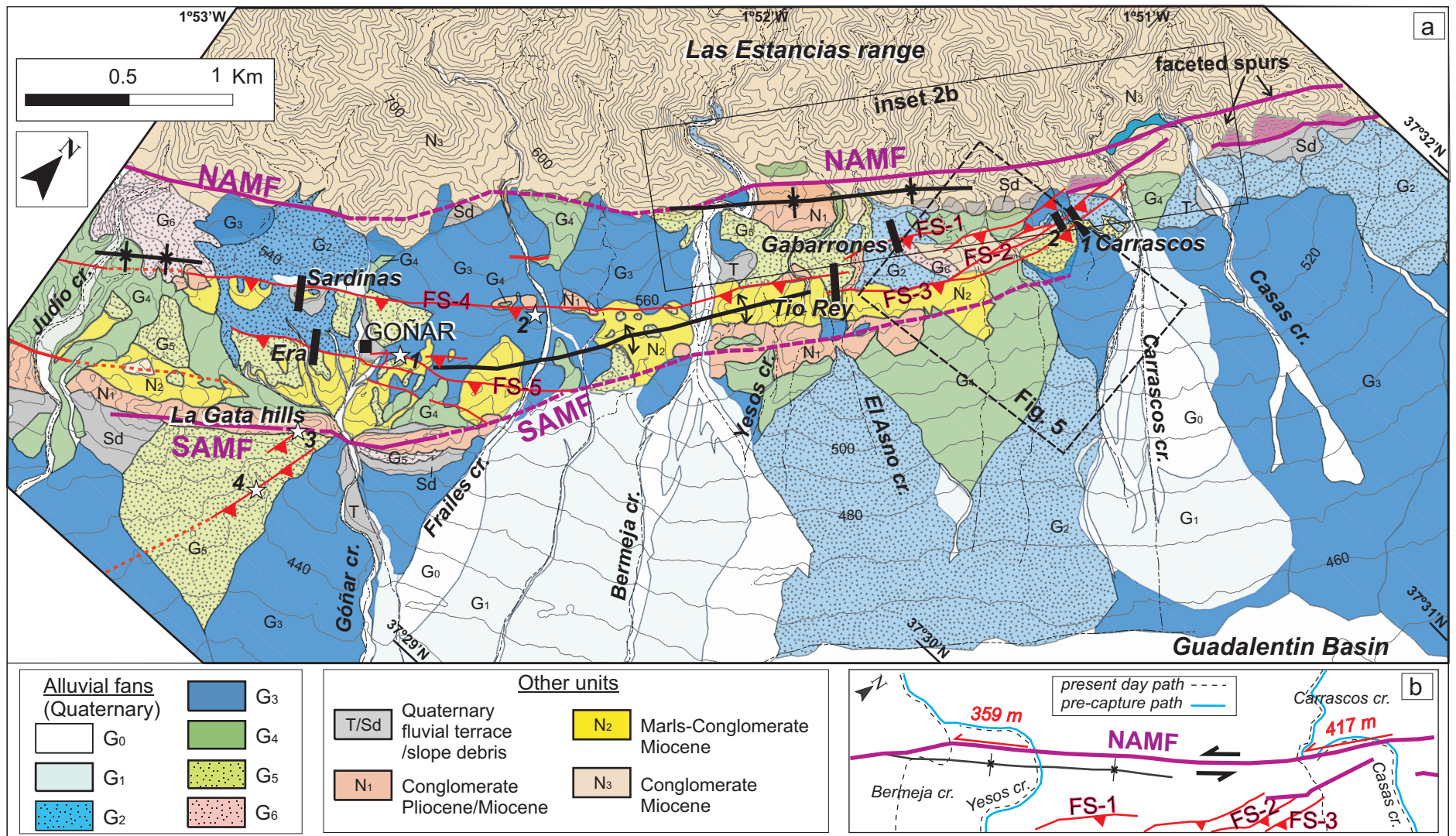


Figure 3
Click here to download Figure: Fig3.pdf

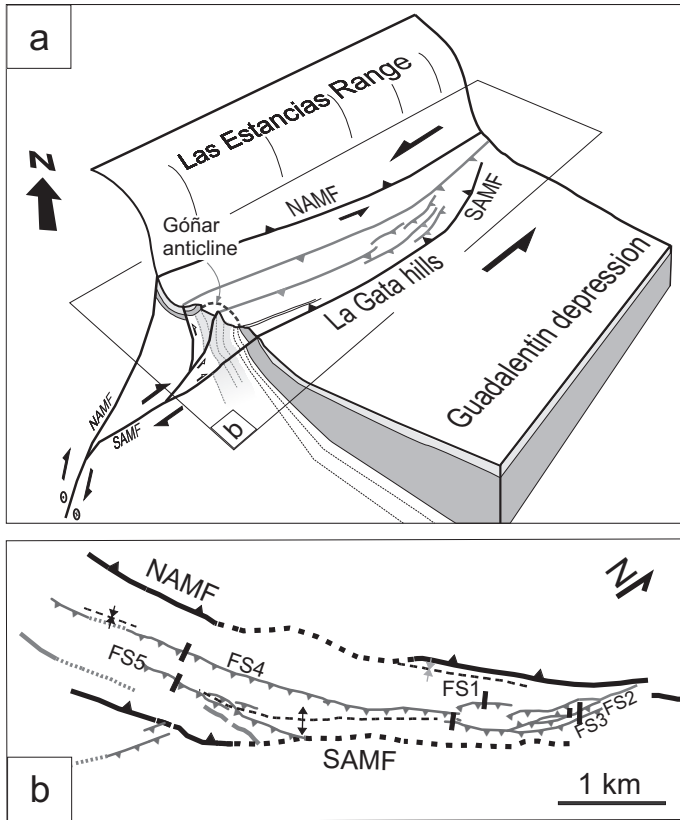
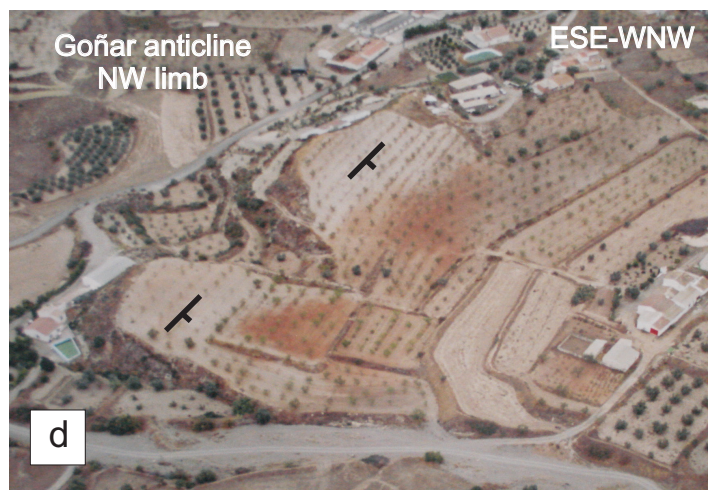
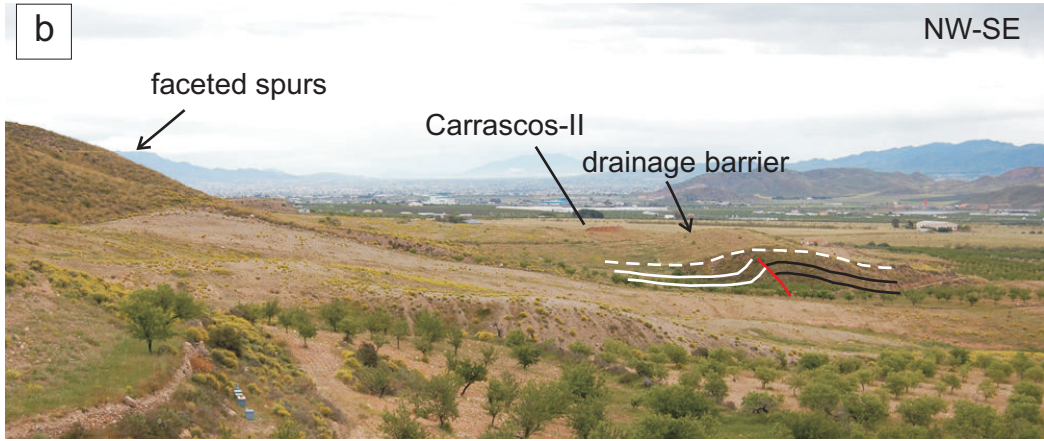
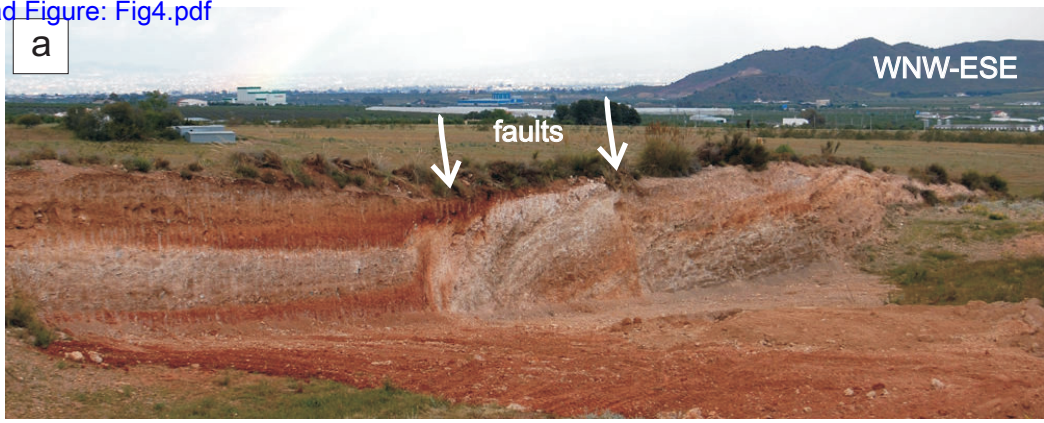


Figure4
Click here to download Figure: Fig4.pdf



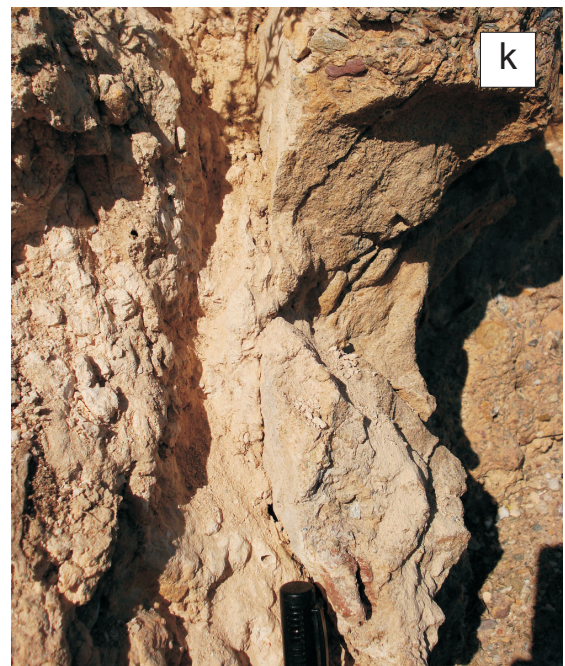
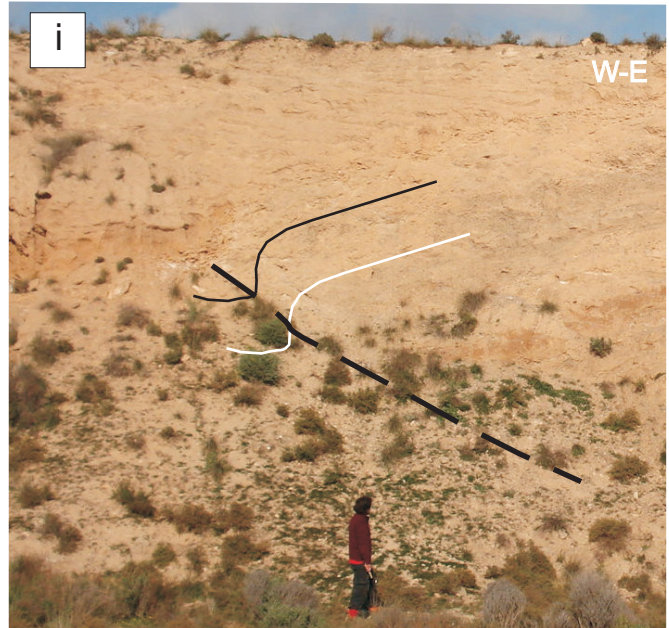
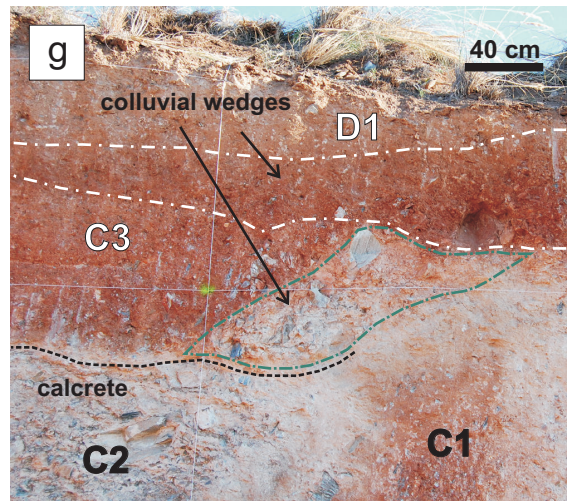
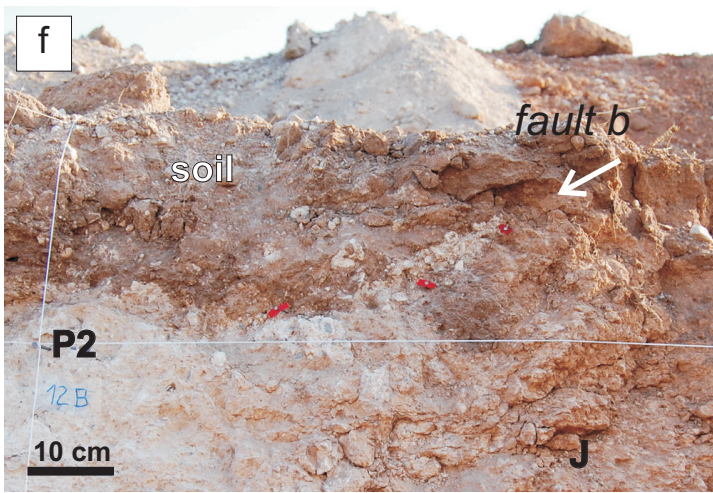


Figure5
Click here to download Figure: Fig5.pdf

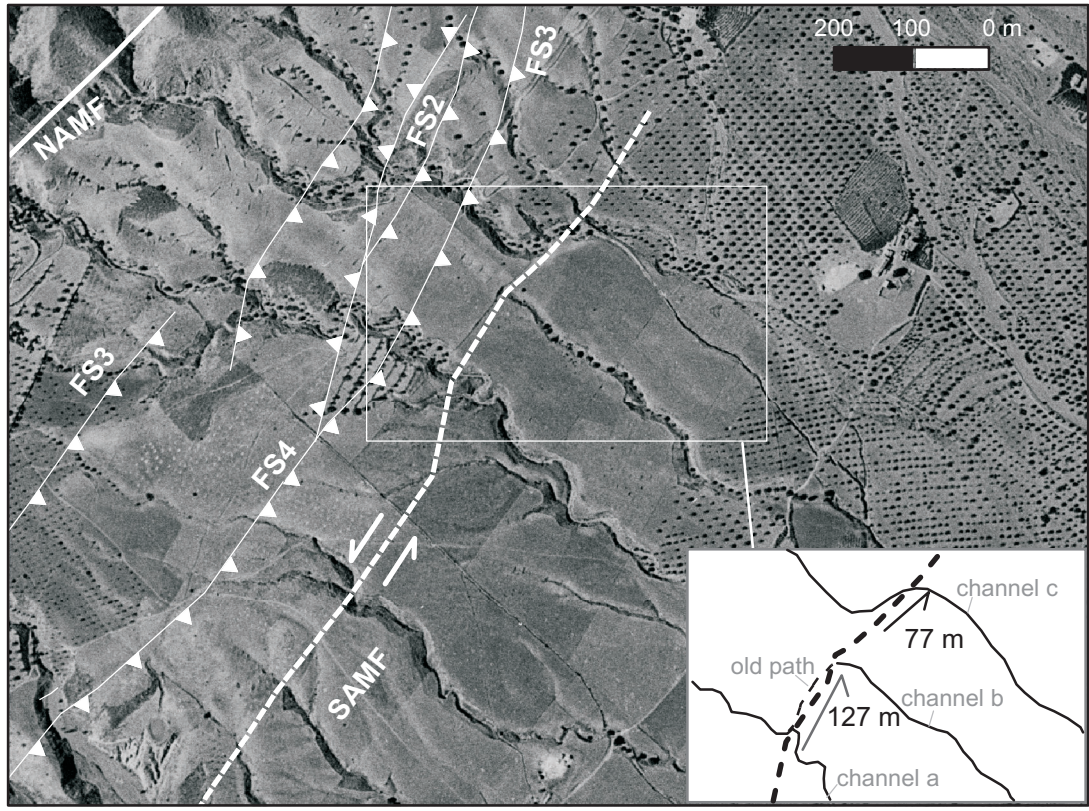
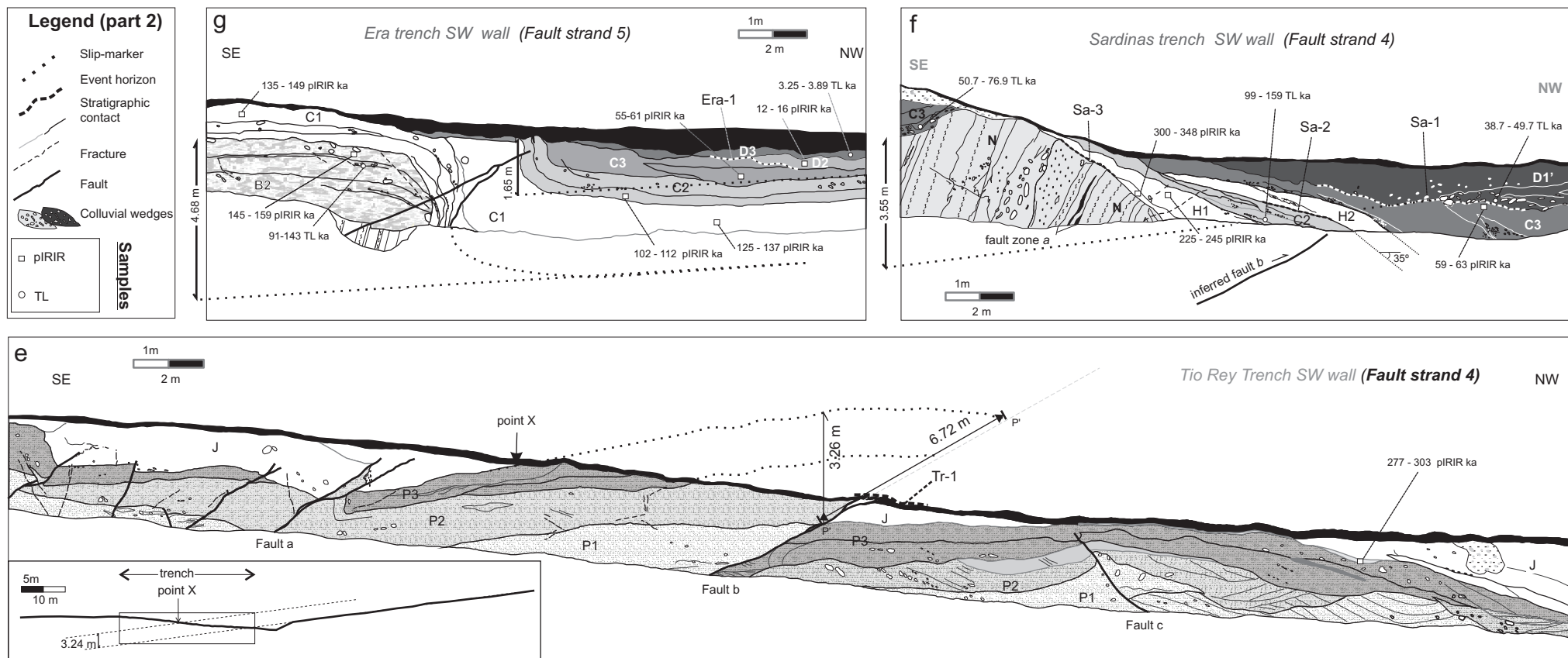


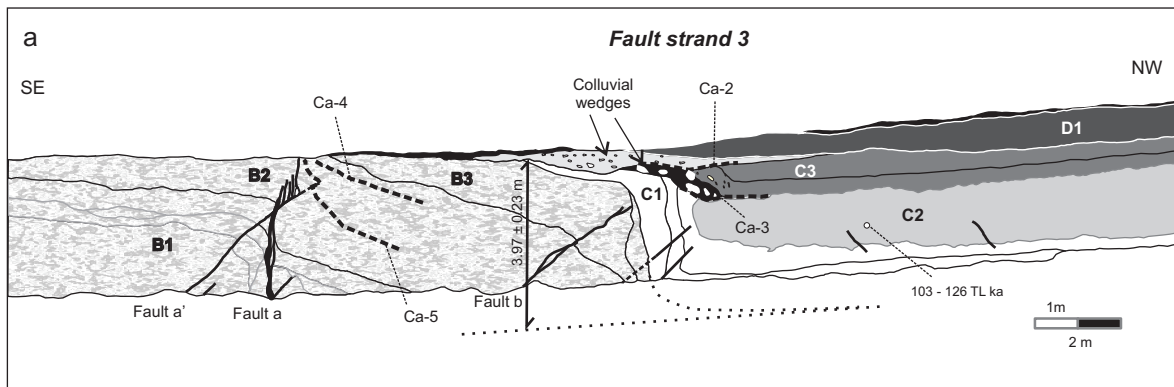
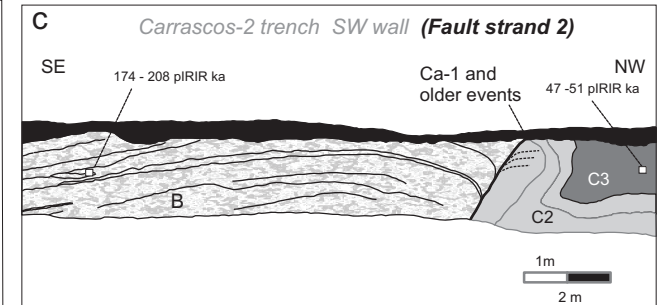
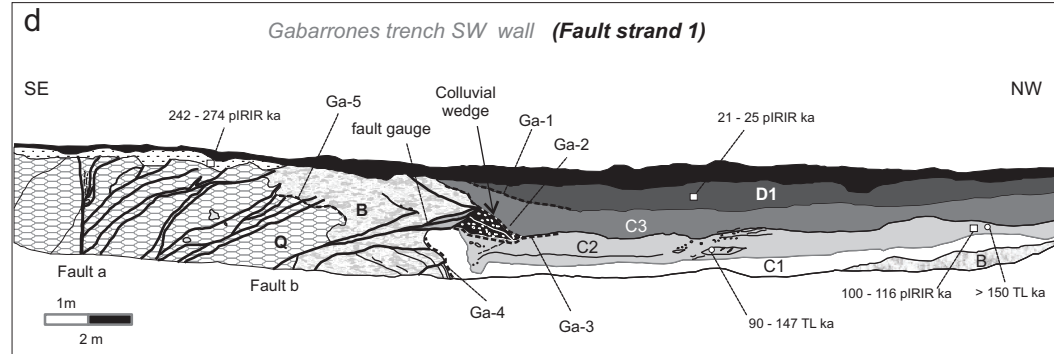
Figure 6

[Click here to download Figure: Fig.6.pdf](#)



Legend (part 1)

<p>Present-day soil</p> <p>Regolith</p> <p>D3 Dark brown matrix supported rounded heterometric gravels, composed of schist and quartzite clasts, varying between a few millimeters and 5 cm in size. Matrix made of sand and silt.</p> <p>D2 Brown matrix supported rounded heterometric gravels, composed of schist and minor quartzite clasts, varying between a few millimeters and 10 cm in size. Matrix made of sand and silt. Strongly affected by burrowing.</p> <p>D1 Brown matrix supported rounded heterometric gravels, composed of schist and minor quartzite clasts, varying between a few millimeters and 10 cm in size. Matrix made of sand and silt. Strongly affected by burrowing.</p> <p>C3 Reddish matrix supported subangular heterometric gravels, with sparse carbonation. Occasionally, the units have conglomeratic lenses of clast-supported rounded clasts. Clasts lithologies vary from schist, quartzite to minor marble. Sub-units C1 and C3 have several calcrete levels, are pumpkin to white in color with clasts smaller than 3 cm. Sub-unit C2 have a characteristic red to strong red color and clasts up to 15 cm diameter.</p> <p>C2</p> <p>C1</p>	<p>H White fine sand and silt with local lensoidal layers of fine gravels.</p> <p>B2-3 Gray and light red sub-rounded matrix supported and layered of heterometric gravels of silicate lithologies mainly medium to fine sized, locally coarse. It is characterized by sparse calcification and areas of rubbification around remains of roots.</p> <p>B(B1) Gray sub-rounded clast-supported and layered homometric micro-conglomerate and gravels of silicate lithologic mainly medium to fine sized, locally coarse. In Gabarrones trench, the unit is locally matrix-supported.</p> <p>H Clast supported heterometric conglomerates made of quartzite and schist subangular clasts of <10 cm diameter. Gray color. Many clasts are broken. A regolith is developed on this unit.</p> <p>J Light brown clast to matrix supported heterometric gravels made of quartzite and schist rounded clasts of <10 cm diameter. Locally, high concentration of roots and development of calcrete nodules.</p>	<p>P3</p> <p>P2</p> <p>P1</p> <p>Neogene basement Alternating marls and medium to fine well cemented marine conglomerate. Gray-yellow color. The conglomerate are clast-supported, rich in siliceous subangular clasts and have a carbonatic matrix.</p>
--	---	--



Carrascos -1 trench NE wall (flipped)

+ 33.4 m horizontal

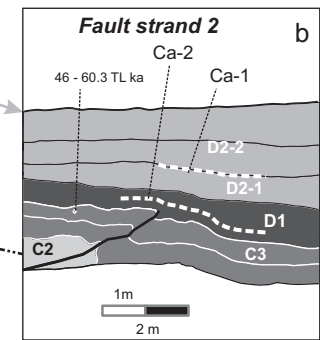


Figure 7

[Click here to download Figure: Fig 7.pdf](#)

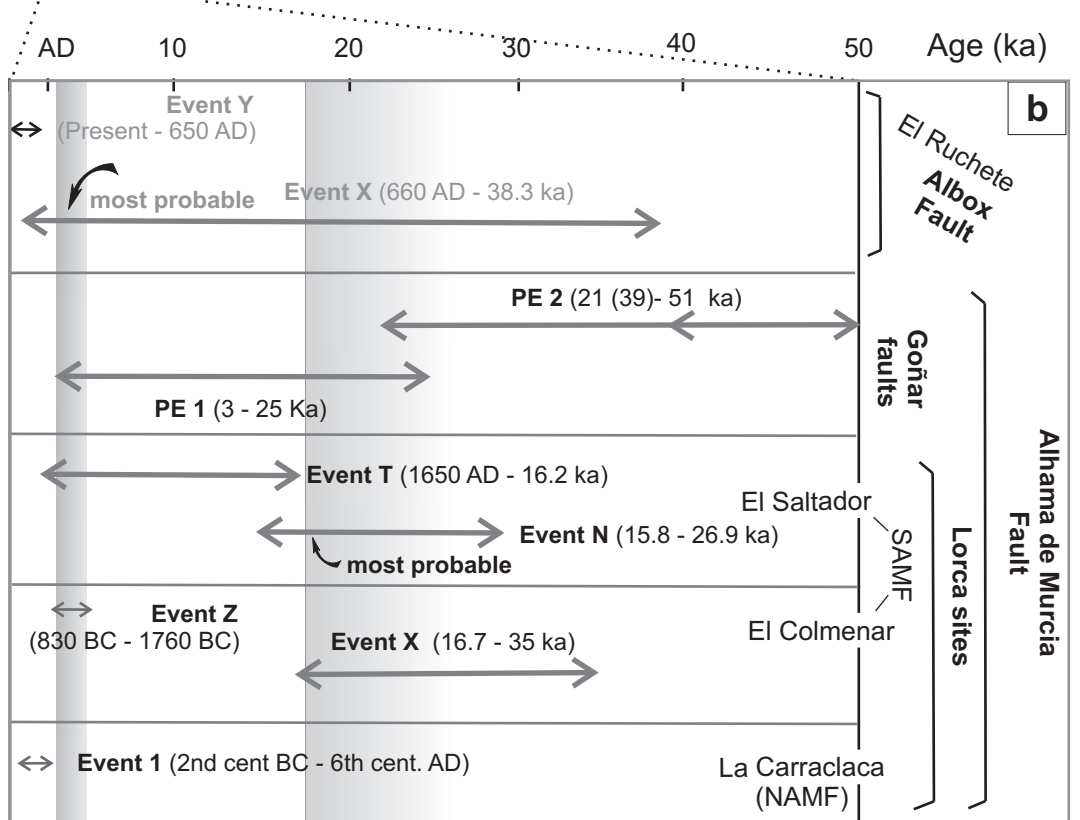
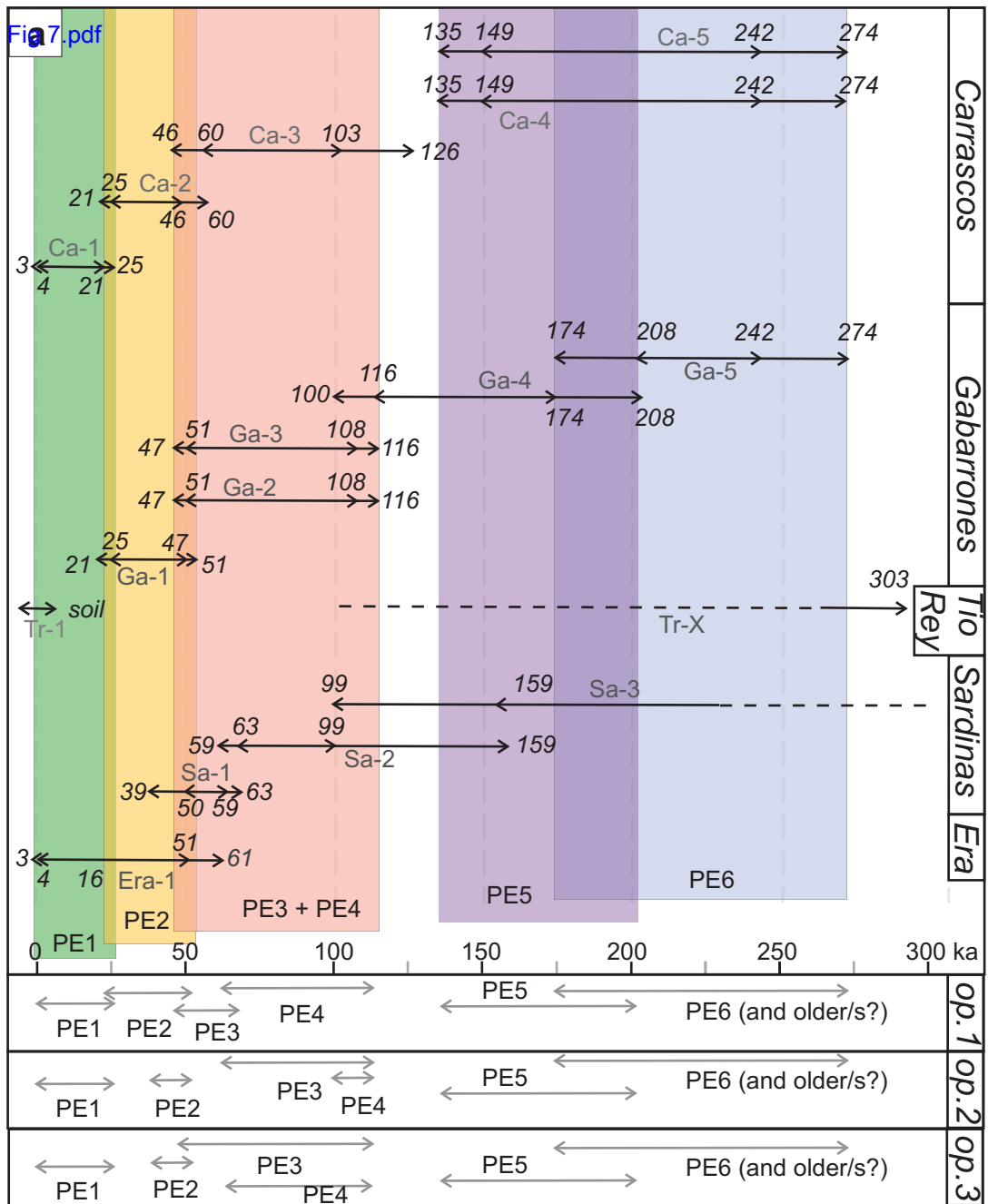


TABLE 1. SUMMARY OF THE PREVIOUS PALAEOSEISMOLOGICAL STUDIES IN THE AREA

Sites	Structure and type of movement	Effects	Slip per event (m) *	Events (age constraint, in ka)	Site	Slip rate (mm/a)
Alhama de Murcia fault, Lorca area	045-065° Lorca-Totana segment. Two main branches. The north branch dips strongly to the NW. The southern branch dips strongly to the SE. Oblique left-lateral and reverse movement	Northern branch: folding of Middle Pleistocene alluvial fans and reverse faulting of a travertine cover.	0.2 – 0.8 V	1) 1.45 – 2.15	La Carraclaca	0,08
		Southern branch: uplift of the SE block. Faulting and blocking of Late Pleistocene and Holocene alluvial fans draining the La Tercia range	~ 0.10 D	Z) 2.78 – 3.08	El Saltador	0.04 – 0.35 V
				X) immediately before 16.7		0.06 – 0.53 S
			0.9 m V	T) just before 0.3	El Colmenar	0.07 – 0.66 N
2.5 m cum. V	N) 26.9 -15.8					
Albox fault , eastern termination	ENE strike, variable dip to the NW. Reverse movement	Folding and faulting of Late Pleistocene and Holocene alluvial fans draining the Las Estancias range	Few cm D	Y) 0.15 – 1.6	El Ruchete	0.01-0.02 V
			≥ 0.5 m V	X) immediately before 1.61	Urcal	0.02-0.04 V
Palomares fault	010-020° Array of normal fault scarps dipping to the E		0.12 V	1) before 126	La Escarihuela	
			0.14 V	2) older than 1)		
			1,8 m	1) 20 - 126		
			2.5 m accumulated in several events	2) several events older than 1)	Aljibejo	

Note: Data derived from Silva et al., 1997; Martínez-Díaz et al., 2003; García-Meléndez, 2000; García-Meléndez et al., 2004; Soler et al., 2003; Masana et al., 2004; Masana et al., 2005.

* The slip rate and slip per event values refer to V, vertical; D, dip; S, strike-slip; N, net displacement.

TABLE 2. DATING RESULTS OF THE STRATIGRAPHIC UNITS SAMPLED

Depositional phase	Unit	Luminescence age (ka)	Sample name and method	General age (ka)	General age (Epoch)
<i>Poorly sorted alluvial fan deposits (fast flood events)</i>					
G2	D3	3.57 ± 0.32	Era-2 (TL)	3.25 – 3.89	Holocene
	D2	14 ± 2	Era-5 (pIRIR)	12 - 16	
	D1	23 ± 2	Gaba-3 (pIRIR)	21 - 25	
	D1'	43.7 +6/-5	Sard-3 (TL)	38.7 - 49.7	
G3	C3	52.4 +7.9/-6.4	Carr-1-2 (TL)	47 - 63	Late Pleistocene
		49 ± 2	Carra-2-1 (pIRIR)		
		58 ± 3	Era-4 (pIRIR)		
		61.9 +15/-11.2	Sard-2 (TL)		
		61 ± 2	Sard-4 (pIRIR)		
		46.3 +6.1/-5.1	Berm - 1 (TL)		
G3-G4	C2	126 +0/-23	Carr-1 (TL)	100 - 125	
		108 ± 8	Gaba-2 (pIRIR)*		
		111+36/-21	Gaba-1 (TL)		
		107 ± 5	Era-3 (pIRIR)*		
		120 +39/-21	Sard-1 (TL)		
G4	C1	142 ± 7	Era-2 (pIRIR)*	125 - 149	Middle-Late Pleistocene
		131 ± 6	Era-0 (pIRIR)*		
<i>Well sorted alluvial fan deposits (channel infill and marginal bars)</i>					
G5	BI-3	152 ± 7	Era-1 (pIRIR)*	>150	
		191 ± 17	Carrascos-3 (pIRIR)*		
G6	Q	258 ± 16	Gaba-1 (pIRIR)* ø	< 242	Middle Pleistocene
G6	H	235 ± 10	Sard-2 (pIRIR)* §	> 400	
		324 ± 24	Sard-1 (pIRIR)* §		
G6	P-J	290 ± 13	Trey-1 (pIRIR)*	277 - 348	

Note:

§ maximum age, ø minimum age, *age could be underestimated for 10-15%

TABLE 3. SUMMARY OF THE EVENTS IDENTIFIED IN THIS STUDY AND THEIR CHRONOLOGICAL CONSTRAINTS

<i>Event</i>	<i>Main evidence and slip and estimated value</i>	<i>Unit postdates/ predates the event</i>	<i>Age range (ka)</i>	<i>Paleo- earthquake</i>	<i>Fault branch</i>
Ga-5	faulting and folding (more than one event)	B/Q	174 - 208 (Carr-2) 242 - 274	6	1
Ca-5	Faulting, 23 ± 2 cm VS	C1 (Top of B)/(Base of B) Q	135 - 149 (Era) / 242- 274 (Gaba)	6	3 (fault <i>a</i>)
Ga-4	faulting	C1/B	100 - 116 / 174 - 208 (Carr-2)	5	1
Ca-4	faulting, ca. 20 cm	C1/Q	135 - 149 (Era) 242- 274 (Gaba)	5	3 (fault <i>a'</i>)
Sa-3	change in sedimentary conditions	C2 (Base of H1)/Neogene	> 99 - 159	4, 5 and/ or 6	4
Ga-3	colluvial wedge, 75 cm VS	C3/C2	47 - 51 (Carr-2) / 108 - 116	4	1
Sa-2	change in sedimentary conditions	C3/C2	59 – 63/99 - 159	3 and/ or 4	4
Ca-3	colluvial wedge, change in sedimentary conditions. VS between 78 ± 6 cm	Contact C3/ C2	46 – 60 / 103 -126	3 or 4	3 (fault <i>b</i>)
Ga-2	faulting, 51 ± 11 cm VS, 116 ± 25 cm NS	C3/ C2	47 - 51 (Carr-2) / 108 - 116	3	1
Ga-1	angular unconformity, 129 ± 3 cm VS	D1/ C3	21- 25/ 47 - 51 (Carr-2)	2	1
Sa-1	angular unconformity, 3.55 m VS (more than one event)	D1/ C3	39 – 50/59 - 63	2 or 3	4
Ca-2	colluvial wedge, angular unconformity 36 ± 4 cm (FS3) VD of base of D1	Within D1 (D2/C3)	21 – 25 (Gaba) / 46 - 60	2	2 and 3
Ca-1	angular unconformity , 23 ± 11 cm VS of D2-1/D2-1	Within D2 (D1/D3)	3 - 4 (Era) / 21 - 25 (Gaba)	1	2
Era-1	angular unconformity	D2/C3	3 – 4/ (12 -16) 51 - 61	1	5
Tr-1	Present-day soil rupture, < 15 cm DS	Present day soil/J	Holocene	1	4

Note: When the age comes from another trench, this has been specified as Carr, Carrascos; Gaba, Gabarrones; Sard, Sardinias. The age defining each paleo-earthquake is marked in bold. N, northern; C, central; S, southern. The slip per event is given as VS (vertical), DS (dip), NS (net).

Table 4

TABLE 4. SLIP RATES DERIVED FROM THE TRENCH ANALYSIS

Site	Marker (fault strand)	Slip (m)				Age range (ka)	Slip rate (mm/a)					
		net	dip	vertical	strike		dip		vertical		Strike (net)	
							min	max	min	max		
<i>Carrascos</i>												
	Base of D1 (FS2)			0.32 – 0.40		21 - 50			0.01	0.02		
	Base of C1 (FS3. fault b)			3.73 – 4.18		125 - 171			0.02	0.03		
	Base of C3 (FS2)			0.98		47 - 63			0.01	0.02		
	Base of C3 (FS3. fault b)			0.84		47 - 63			0.01	0.02		
	Base C3 FS2 + FS3								0.02	0.04		
<i>Gabarrones</i>												
	Base of C3 (FS1)	2.87 - 3.01	2.70 - 2.83	1.26 - 1.31	1.04 - 1.09	47 - 63	0.04	0.06	0.02	0.03	0.02 (0.04)	0.02(0.06)
	Base C3 FS1 + FS2 + FS3								0.04	0.07		
<i>Tio Rey</i>												
	Base of J (FS4. fault b)		5.98 - 7.46	2.90 - 3.62		277 - 348	0.02	0.03	0.01	0.01		
<i>Sardina</i>												
	Base of C3 (FS4)			3.16 - 3.94		47 - 63			0.05	0.08		
<i>Era</i>												
	Base of C3 (FS5)			1.51 - 1.78		47-63			0.02	0.04		
	Base of C2 (FS5)			2.09 – 2.45		100-125			0.02	0.02		
	Base of C1 (FS5)			4.31 – 5.05		125-171			0.02	0.04		
	Base C3 FS4 +FS5								0.07	0.12		
				Strike slip (m)					Strike slip rate (mm/a)			
									min	max		
<i>SAMF</i>	<i>La Gata hills</i>			~ 1000		min 1600					~ 0.62	
	<i>Carrascos/Asno</i>	Creek b		127 ± 6		125 -149		0.81			1.06	
		Creek c		77 ± 10		125 -149		0.45			0.70	
<i>NAMF</i>	<i>Bermeja/Yesos</i>			359 ± 14		max. 750		0.46				
	<i>Carrascos/Casas</i>			417 ± 26		max. 750		0.52				